CHAPTER 5 RESULTS AND DISCUSSION

In this chapter, the results of heat transfer and flow characteristics of HFC-134a during condensation and evaporation inside vertical corrugated tube are presented and discussed.

5.1 Heat transfer and flow characteristics of HFC-134a during evaporation inside vertical corrugated tube

Data are presented in the forms of average heat transfer coefficient and two-phase friction factor. The effects of mass flux, heat flux, and evaporating temperature on the average heat transfer coefficient and two-phase friction factor are investigated.

5.1.1 Average heat transfer coefficient

The average heat transfer coefficient obtained from the smooth tube is compared with the results calculated from the correlations proposed by Shah (1982), Gungor and Winterton (1986) and Kandlikar (1990). As shown in Figure 5.1, these correlations can describe almost all of the heat transfer coefficient within 20%.

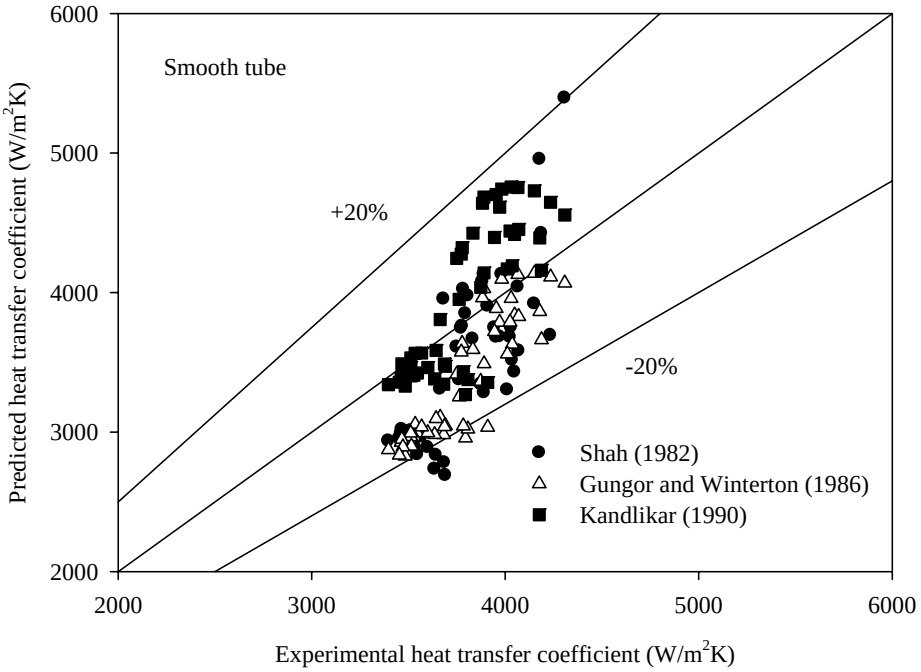

Figure 5.1 Comparison of experimental evaporation heat transfer coefficient data with existing correlations.

5.1.1.1 Effect of mass flux

The effect of the mass flux on the average heat transfer coefficient can be observed from Figs. 5.2-5.6. They show the variations of the average heat transfer coefficient as a function of average quality at constant saturation temperature and heat flux for different mass fluxes of 200, 300, and 400 kg/m^{2}s. The average quality is shown in the present work. It is averaged from the inlet quality and outlet quality of the test section. During evaporation, the liquid film thickness decreases gradually, and the thermal resistance is therefore decreased, resulting in an increase in the heat transfer rate. As a result, the average heat transfer coefficient increases with increasing average quality. In addition, the average heat transfer coefficient increases with a rise in the mass flux. This is because the increase in the mass flux also increases the velocity of the vapor and liquid film and the flow turbulence as a result of enhancing the convective heat transfer.

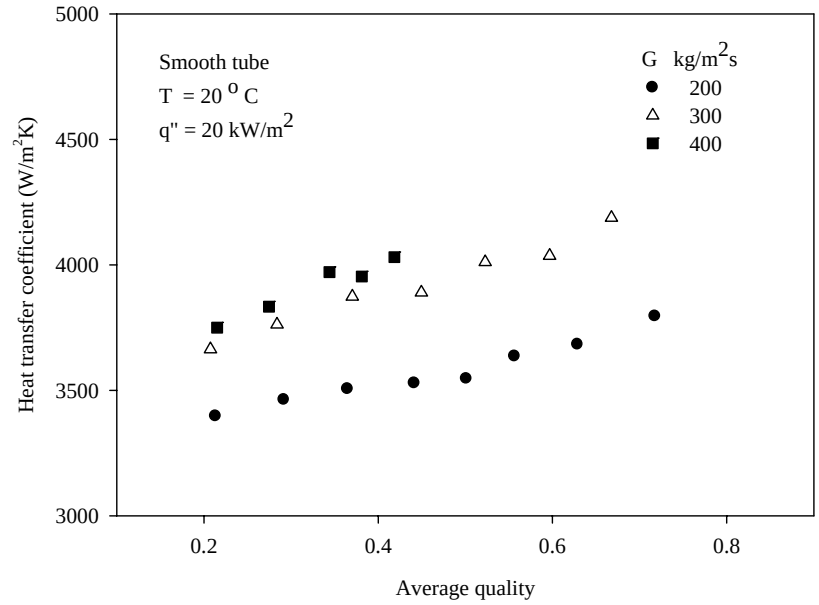

Figure 5.2 Effect of mass flux on evaporation heat transfer coefficient for a smooth tube.

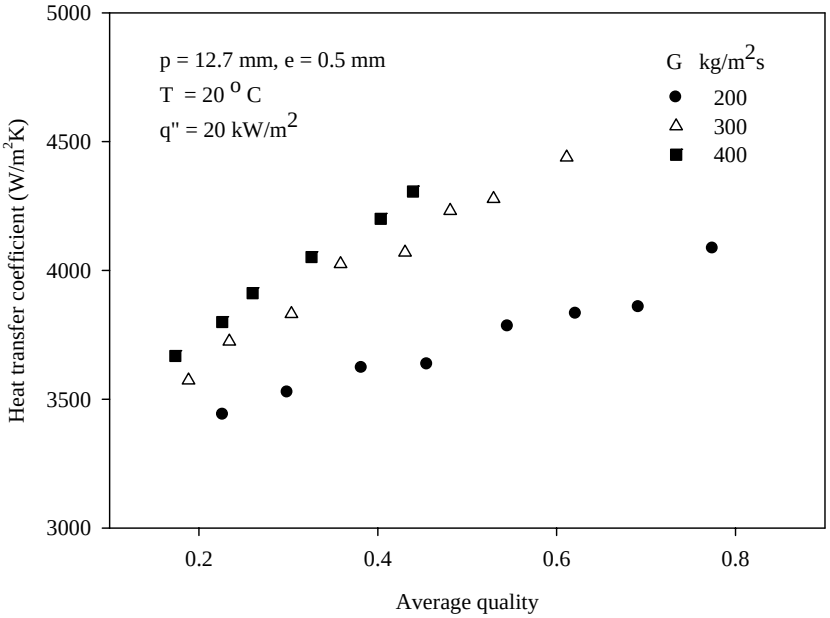

Figure 5.3 Effect of mass flux on evaporation heat transfer coefficient for a tube with p = 12.7 mm and e = 0.5 mm.

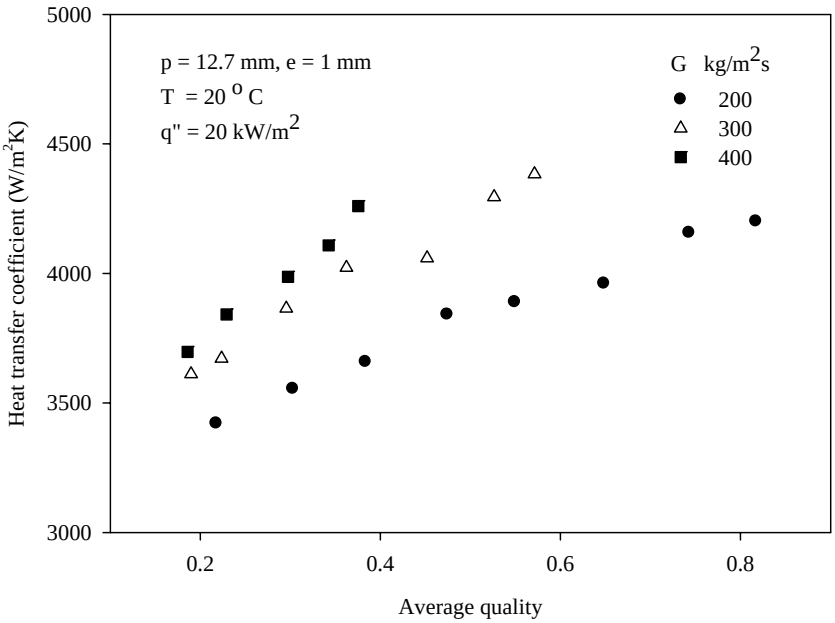

Figure 5.4 Effect of mass flux on evaporation heat transfer coefficient for a tube with p = 12.7 mm and e = 1 mm.

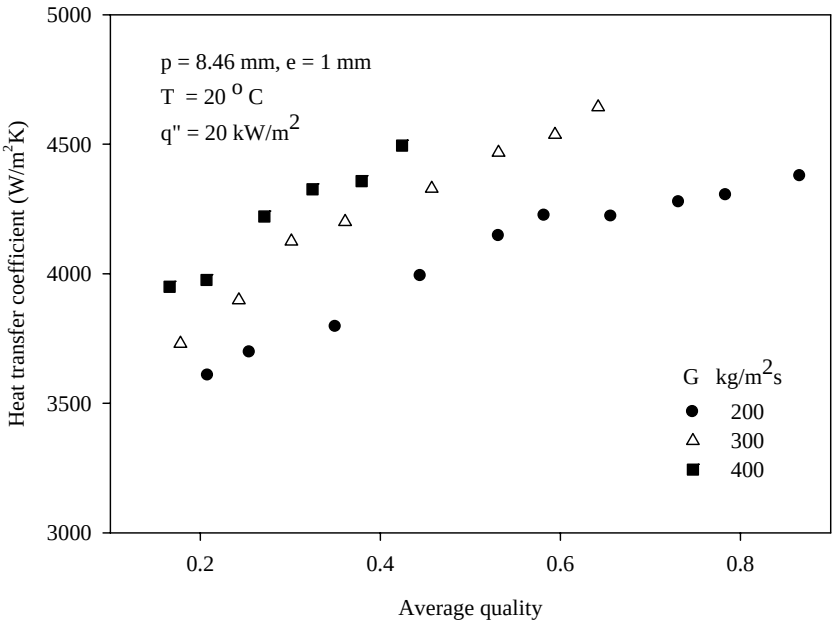

Figure 5.5 Effect of mass flux on evaporation heat transfer coefficient for a tube with p = 8.46 mm and e = 1 mm.

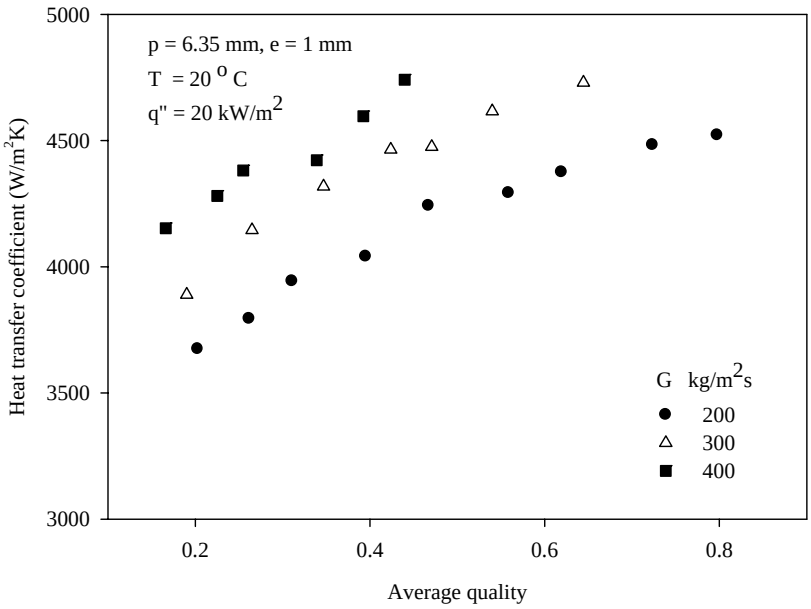

Figure 5.6 Effect of mass flux on evaporation heat transfer coefficient for a tube with p = 6.35 mm and e = 1 mm.

5.1.1.2 Effect of heat flux

Figs. 5.7-5.11 show the relationship between average heat transfer coefficient and average quality at constant mass flux and saturation temperature. These figures show the results of three different values of heat flux: 20, 25, and 30 kW/m^2. In this experiment, as the heat flux increases, the heat transfer coefficient also increases. The increase in heat transfer rate which is caused by the increase of the heat flux causes the number of bubbles to increase. These bubbles can induce turbulent flow in the liquid film, resulting in increased heat transfer coefficient. At low or moderate quality, the heat transfer enhancement is more remarkable than at high quality. This is due to the fact that the nucleate boiling mechanism is much stronger than the effect of force convective at low quality. On the other hand, it becomes weaker at high quality.

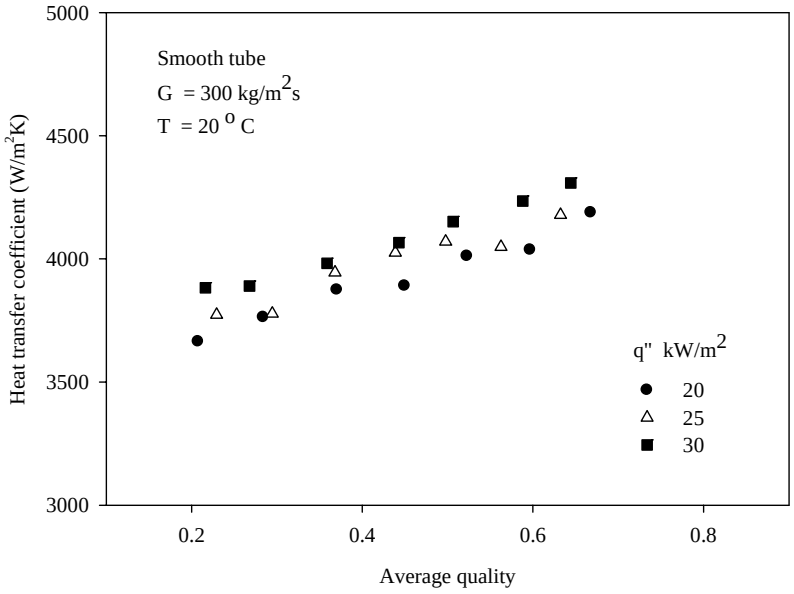

Figure 5.7 Effect of heat flux on evaporation heat transfer coefficient for a smooth tube.

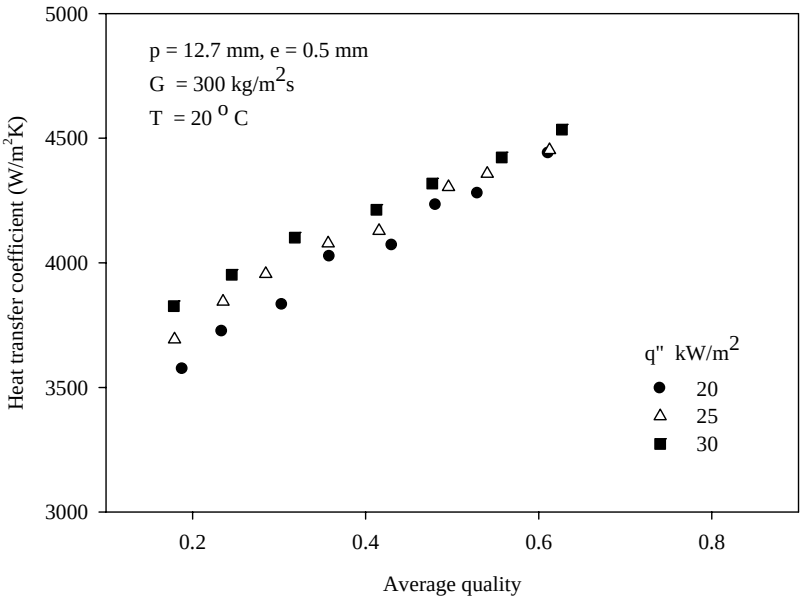

Figure 5.8 Effect of heat flux on evaporation heat transfer coefficient for a tube with p = 12.7 mm and e = 0.5 mm.

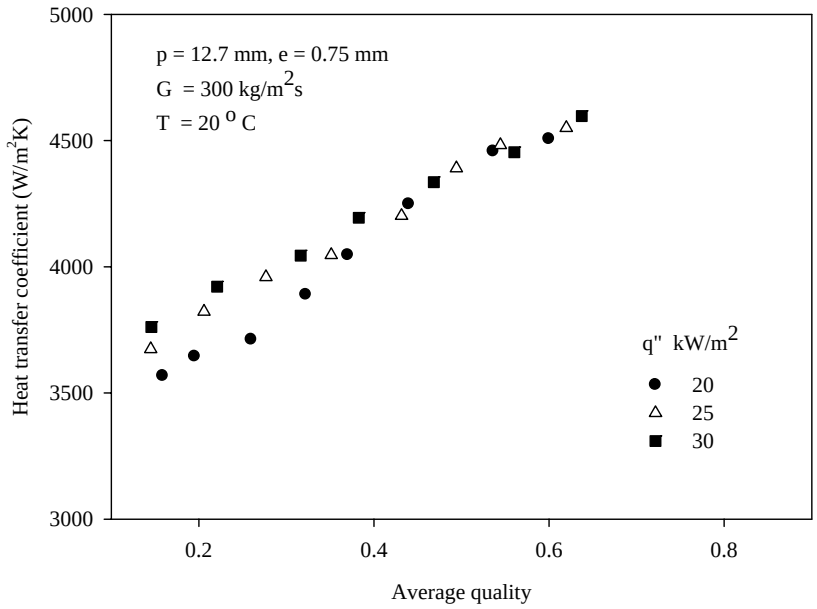

Figure 5.9 Effect of heat flux on evaporation heat transfer coefficient for a tube with p = 12.7 mm and e = 0.75 mm.

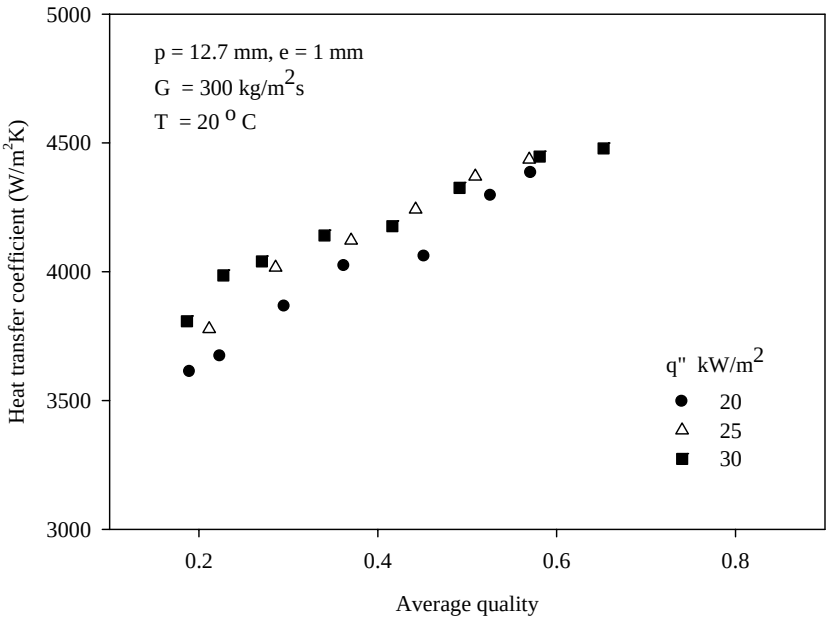

Figure 5.10 Effect of heat flux on evaporation heat transfer coefficient for a tube with p = 12.7 mm and e = 1 mm.

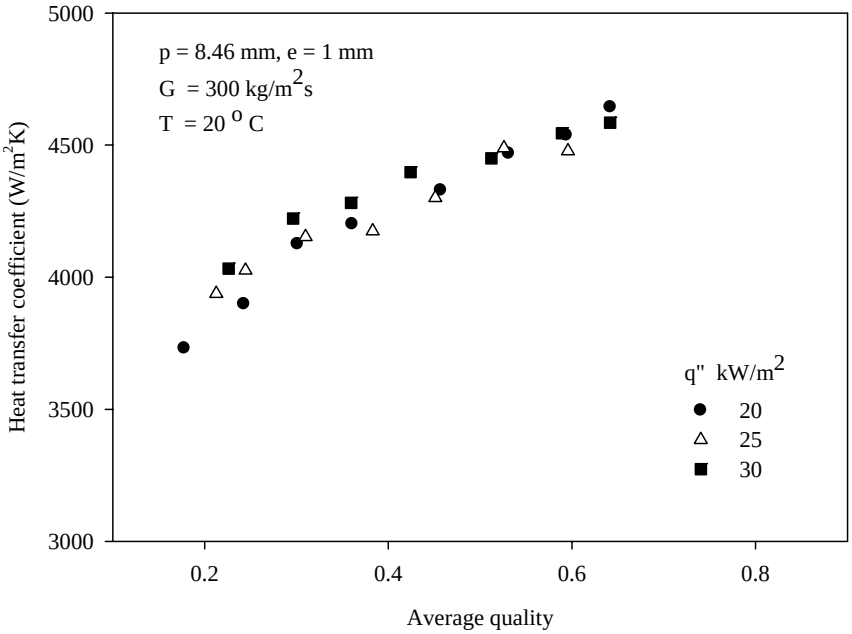

Figure 5.11 Effect of heat flux on evaporation heat transfer coefficient for a tube with p = 8.46 mm and e = 1 mm.

5.1.1.3 Effect of saturation temperature

Figs. 5.12-5.16 present the variation of average heat transfer coefficient with average quality at constant mass flux and heat flux for different saturation temperatures of 10, 15, and 20 °C. It can be seen that the heat transfer coefficient is changed by a relatively small amount with increasing evaporating temperature.

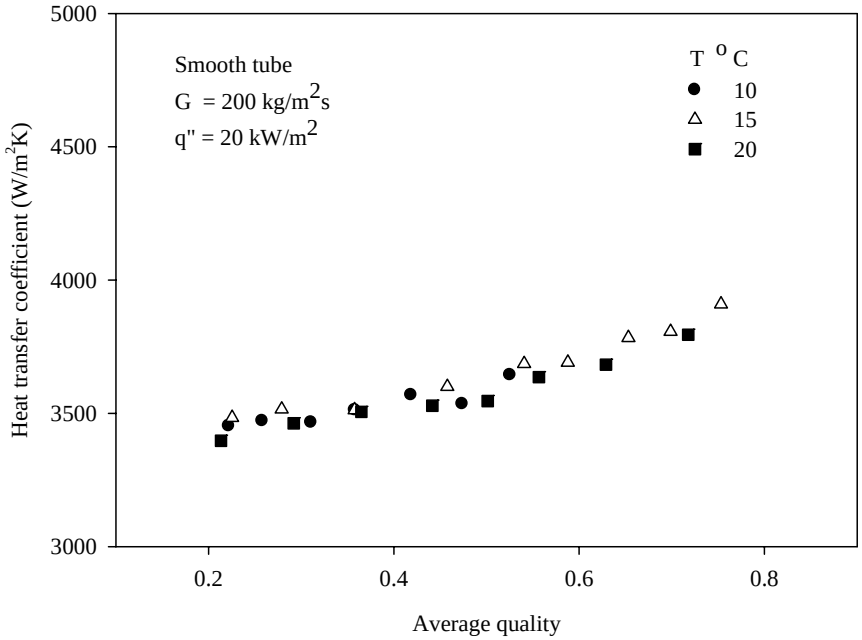

Figure 5.12 Effect of saturation temperature on evaporation heat transfer coefficient for a smooth tube.

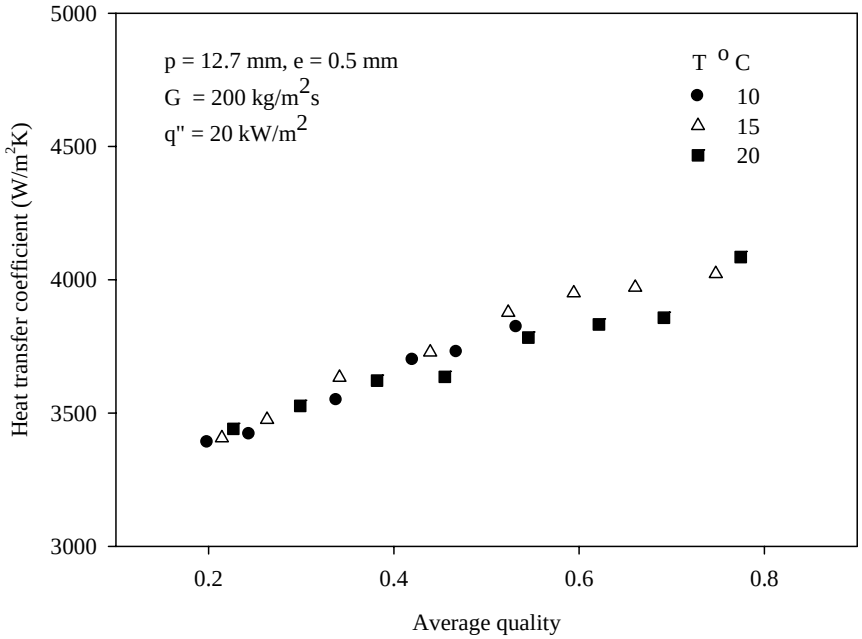

Figure 5.13 Effect of saturation temperature on evaporation heat transfer coefficient for a tube with p = 12.7 mm and e = 0.5 mm.

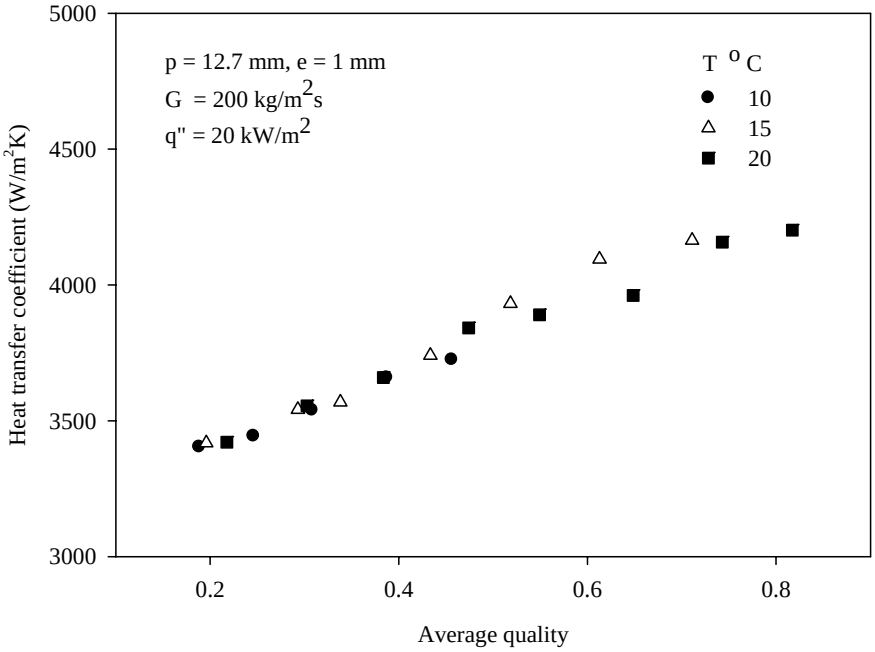

Figure 5.14 Effect of saturation temperature on evaporation heat transfer coefficient for a tube with p = 12.7 mm and e = 1 mm.

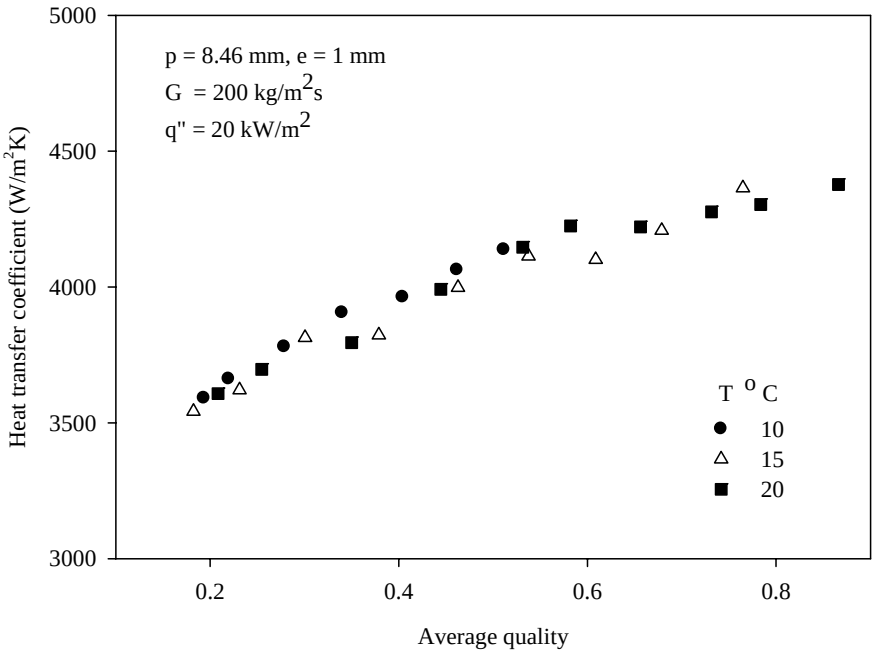

Figure 5.15 Effect of saturation temperature on evaporation heat transfer coefficient for a tube with p = 8.46 mm and e = 1 mm.

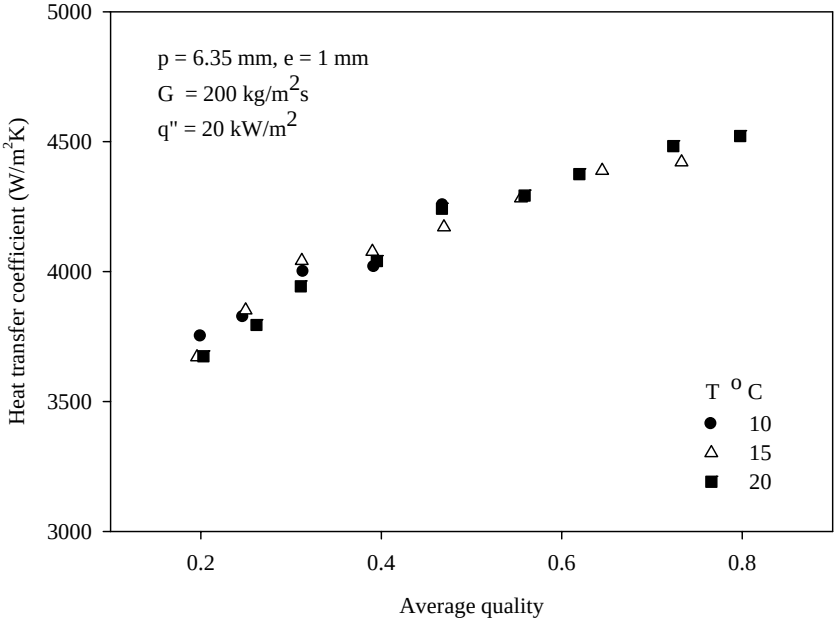

Figure 5.16 Effect of saturation temperature on evaporation heat transfer coefficient for a tube with p = 6.35 mm and e = 1 mm.

5.1.1.4 The comparison between smooth and corrugated tubes

The comparisons of the evaporative heat transfer coefficient between the smooth and the corrugated tubes are shown in Figs. 5.17-5.29. These figures reveal that the heat transfer coefficient for the corrugated tubes is higher than that for the smooth tube. This is due to an increase in the heat transfer area and more turbulence induced by corrugated surface. The corrugated tubes may provide periodic redevelopment of the boundary layers, causing more effective heat transfer. In other words, thermal boundary layer inside a corrugated tube became thinner than that inside a smooth tube (Bilen et al. 2009). Additionally, the effect of corrugation on the heat transfer coefficient is weak in low vapor quality region. On the other hand, the effect of corrugation becomes stronger at high vapor quality. This can be explained by the fact that when the liquid film thickness is close to the corrugation depth, the periodic liquid wave caused by

corrugated pitch produces an unstable liquid flow which maximizes thermal efficiency and turbulent effects (Yun et al. 2002).

The effects of different corrugation pitches with a constant corrugation depth of 1 mm on the enhancement of heat transfer coefficient are also shown in Figs. 5.17-5.23. It is observed that the heat transfer coefficient increases with the decrease of corrugation pitch. This is because the tube with lower corrugation pitch generates more turbulence of the fluid flow and increases heat transfer area. Hence, the highest heat transfer coefficient is caused by the tube with the lowest corrugation pitch. The maximum heat transfer enhancement is obtained up to 22% for a pitch of 6.35 mm, 16% for a pitch of 8.46 mm, and 11% for a pitch of 12.7 mm in comparison with the smooth tube at the mass flux of 200 kg/m^{2}s, the heat flux of 20 kW/m^2, and the saturation temperature of 20 °C.

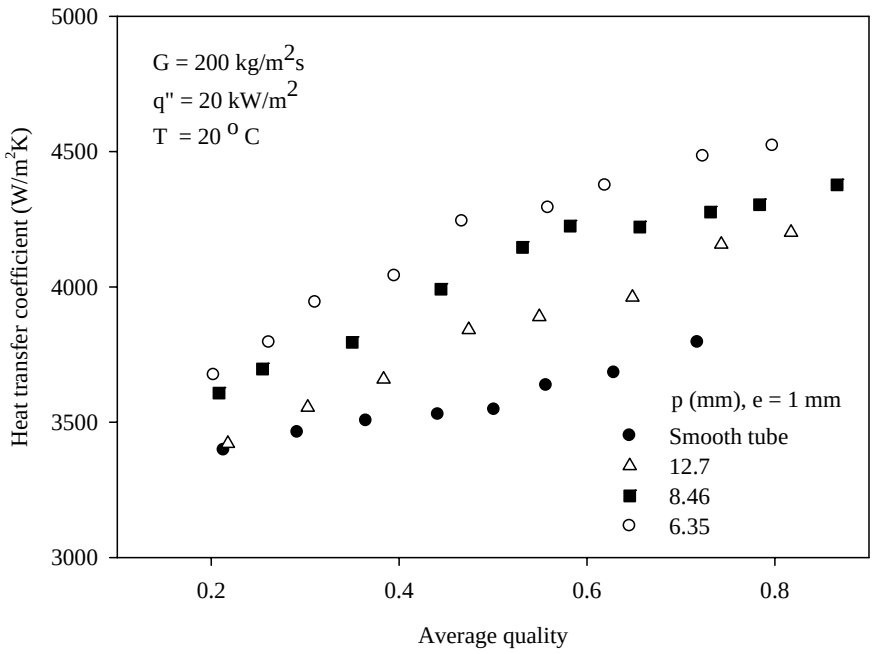

Figure 5.17 Effect of corrugation pitch on evaporation heat transfer coefficient for G = 200 kg/m^{2}s, q" = 20 kW/m^2 and T = 20 °C.

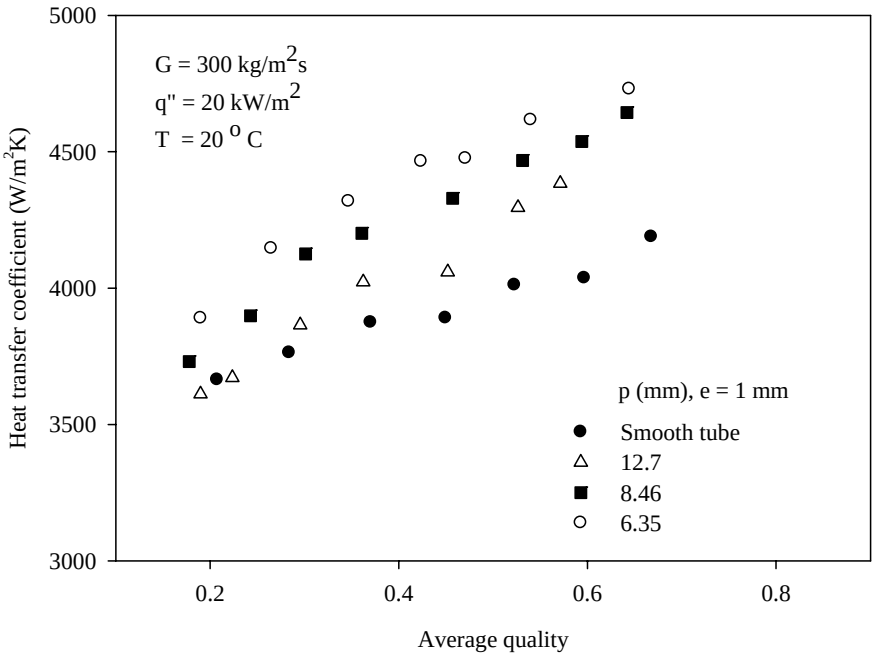

Figure 5.18 Effect of corrugation pitch on evaporation heat transfer coefficient for G = 300 kg/m^{2}s, q" = 20 kW/m^2 and T = 20 °C.

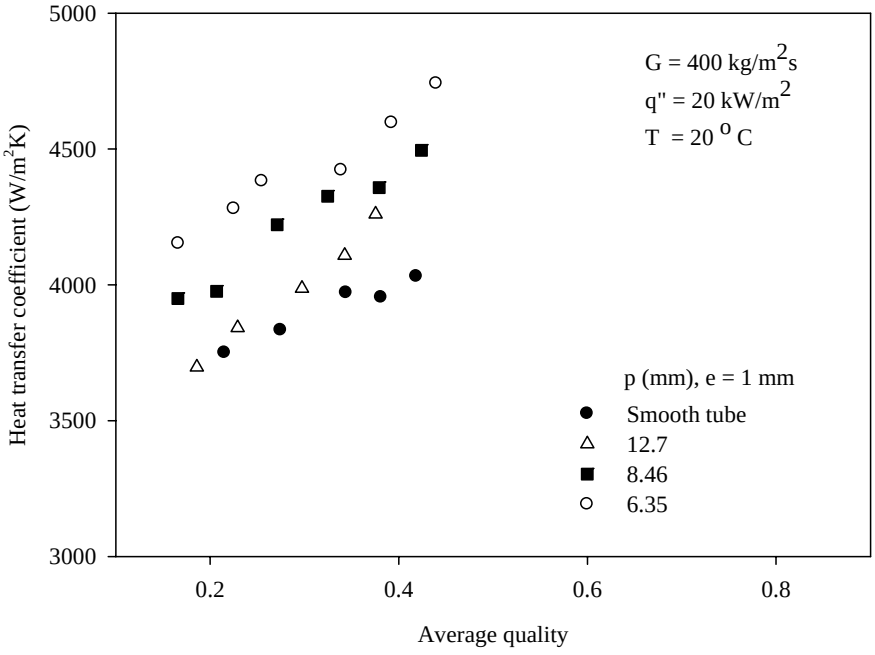

Figure 5.19 Effect of corrugation pitch on evaporation heat transfer coefficient for G = 400 kg/m^{2}s, q" = 20 kW/m^2 and T = 20 °C.

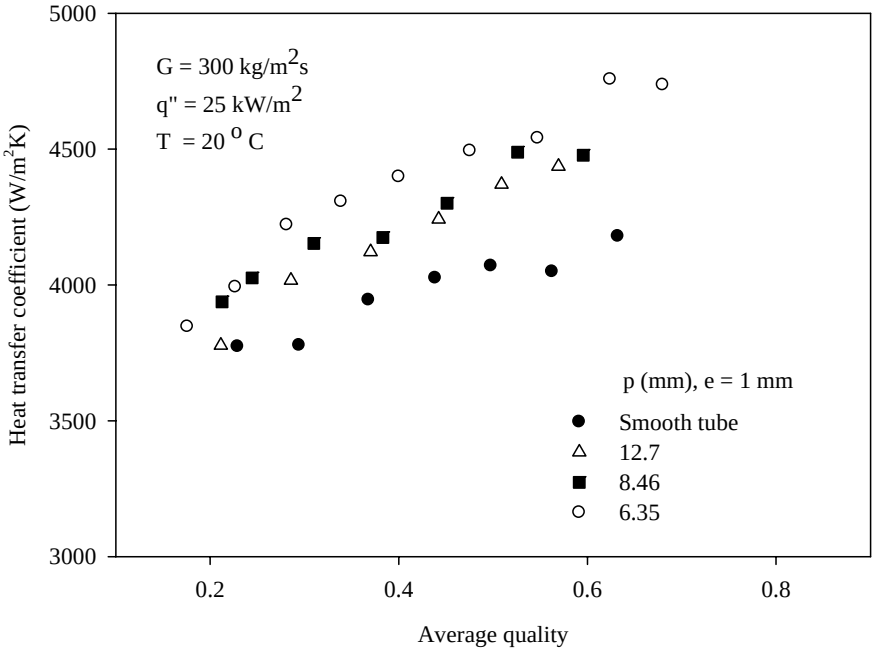

Figure 5.20 Effect of corrugation pitch on evaporation heat transfer coefficient for G = 300 kg/m^{2}s, q" = 25 kW/m^2 and T = 20 °C.

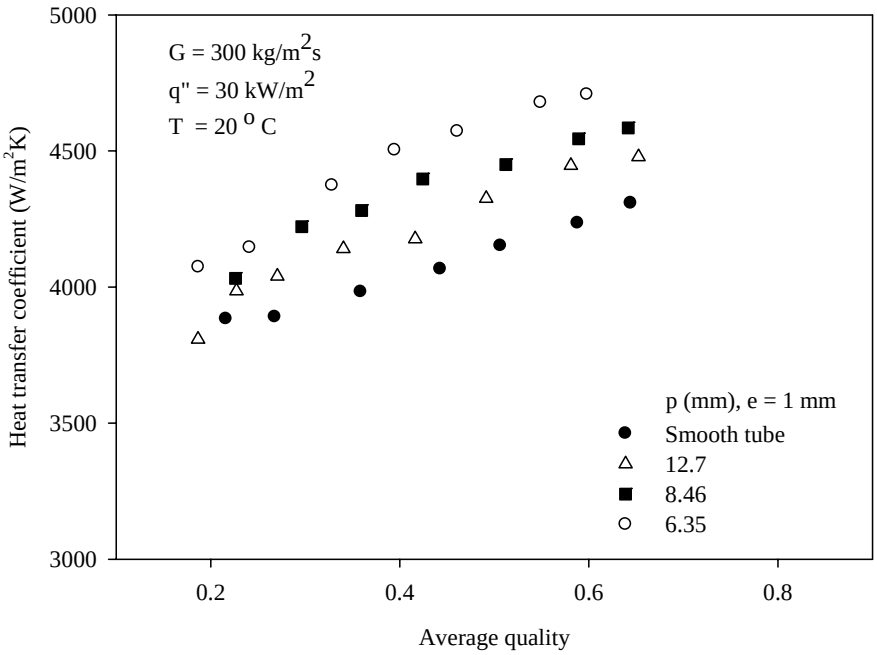

Figure 5.21 Effect of corrugation pitch on evaporation heat transfer coefficient for G = 300 kg/m^{2}s, q" = 30 kW/m^2 and T = 20 °C.

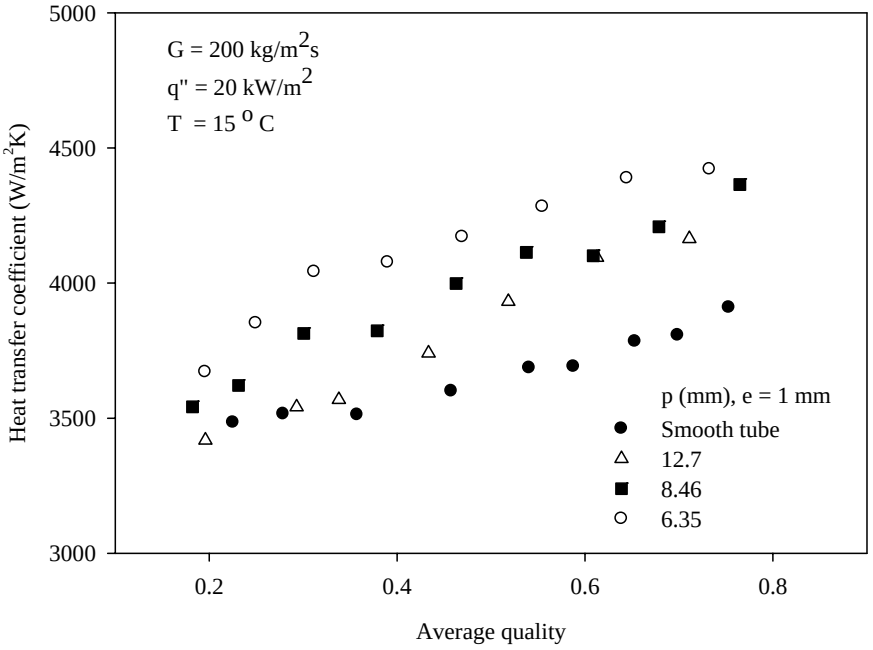

Figure 5.22 Effect of corrugation pitch on evaporation heat transfer coefficient for G = 200 kg/m^{2}s, q" = 20 kW/m^2 and T = 15 °C.

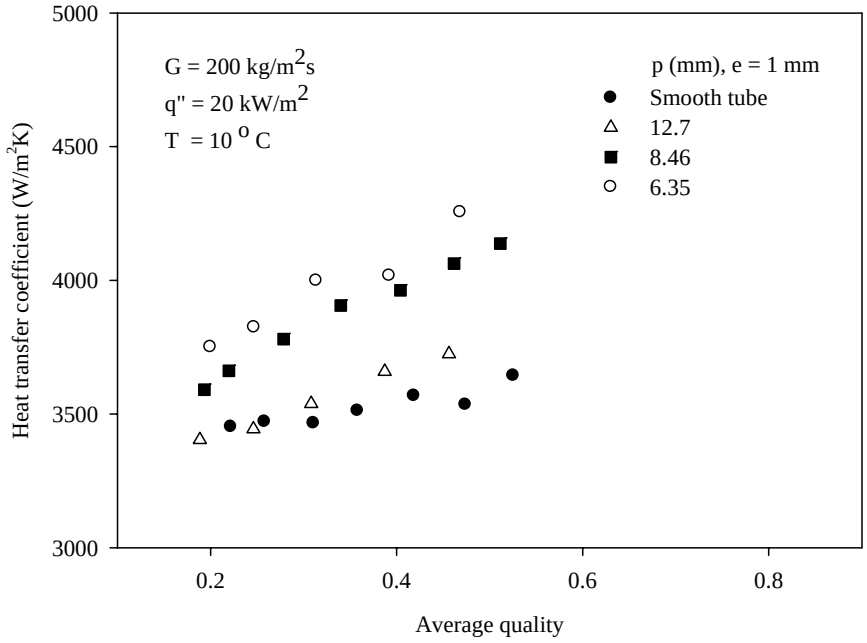

Figure 5.23 Effect of corrugation pitch on evaporation heat transfer coefficient for G = 200 kg/m^{2}s, q" = 20 kW/m^2 and T = 10 °C.

Figs. 5.24-5.29 demonstrate the effect of the corrugation depth on the heat transfer coefficient. It is found that the corrugation depth has a slight effect on the heat transfer coefficient. The maximum heat transfer coefficient of the corrugated tube is up to 11% higher than that of the smooth tube at the mass flux of 200 kg/m^{2}s, heat flux of 20 kW/m^2, and saturation temperature of 20 °C.

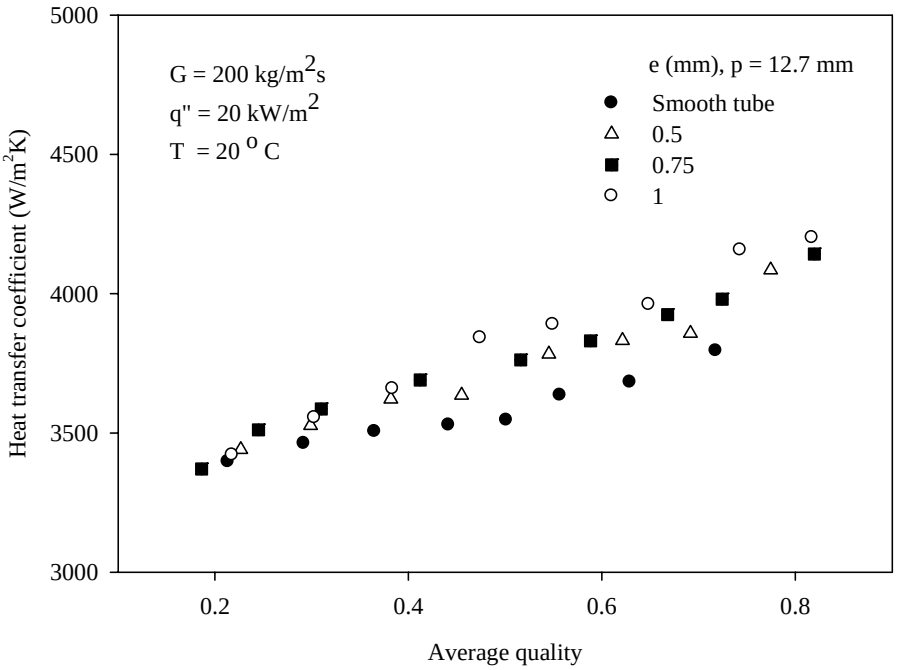

Figure 5.24 Effect of corrugation depth on evaporation heat transfer coefficient for G = 200 kg/m^{2}s, q" = 20 kW/m^2 and T = 20 °C.

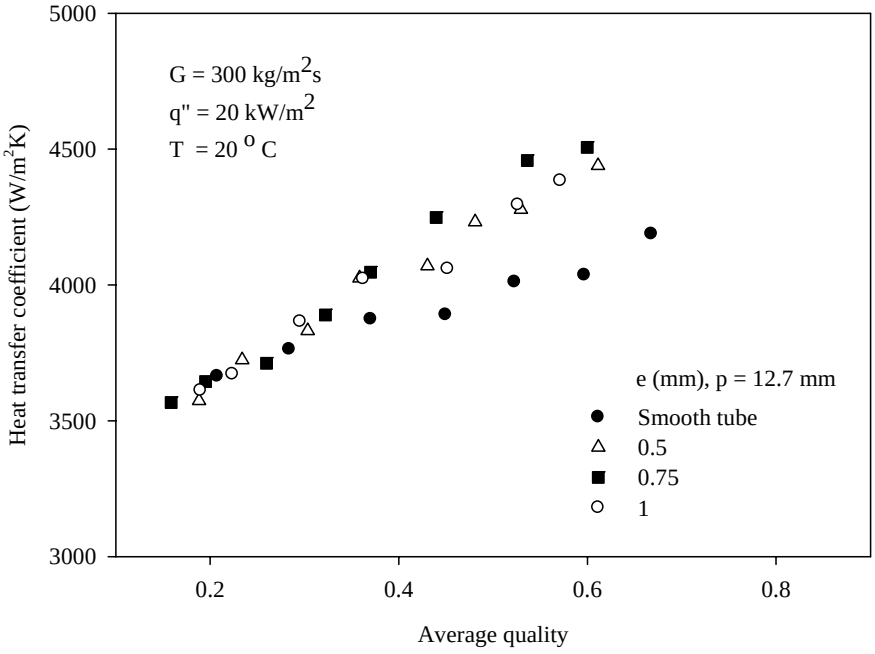

Figure 5.25 Effect of corrugation depth on evaporation heat transfer coefficient for G = 300 kg/m^{2}s, q" = 20 kW/m^2 and T = 20 °C.

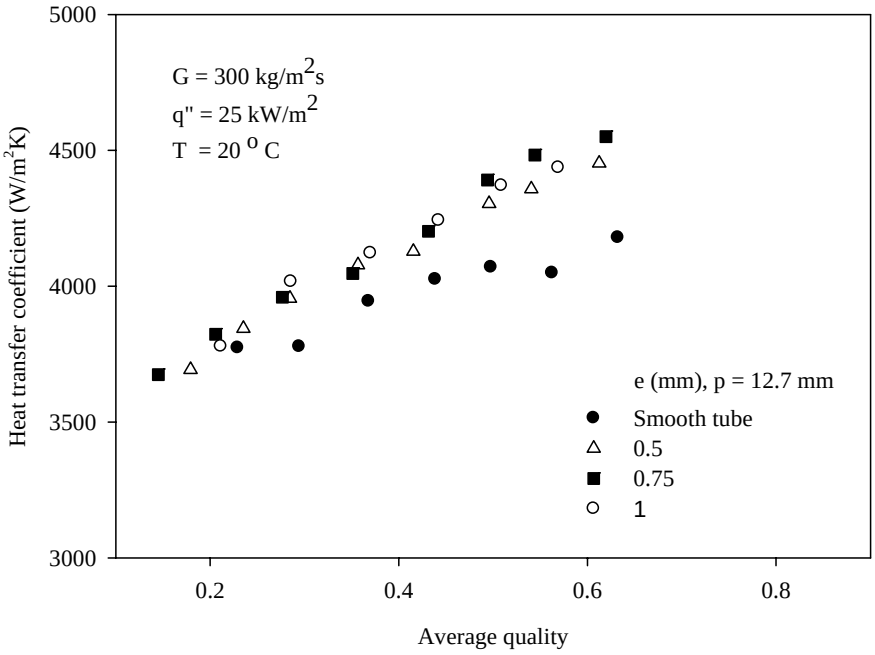

Figure 5.26 Effect of corrugation depth on evaporation heat transfer coefficient for G = 300 kg/m^{2}s, q" = 25 kW/m^2 and T = 20 °C.

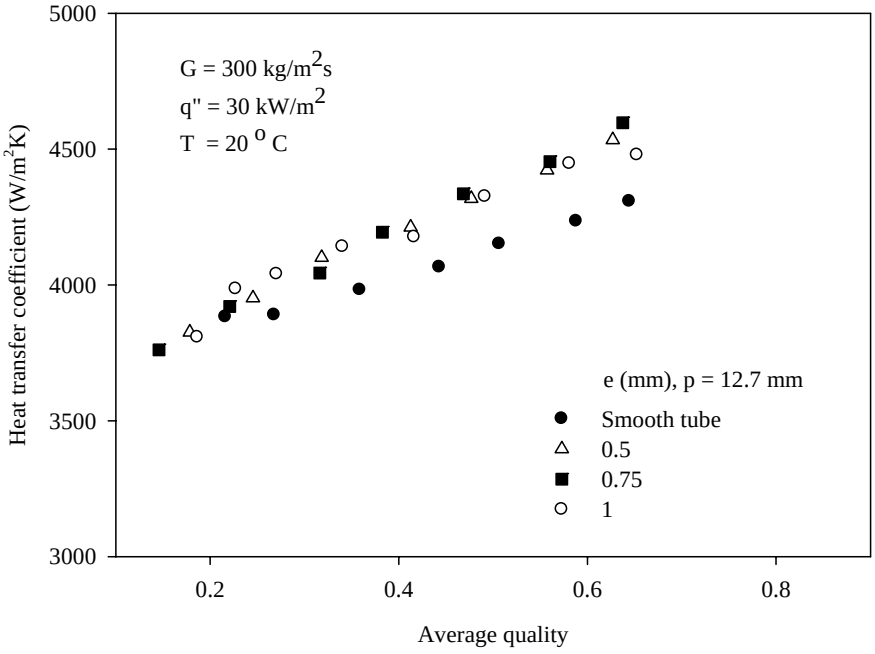

Figure 5.27 Effect of corrugation depth on evaporation heat transfer coefficient for G = 300 kg/m^{2}s, q" = 30 kW/m^2 and T = 20 °C.

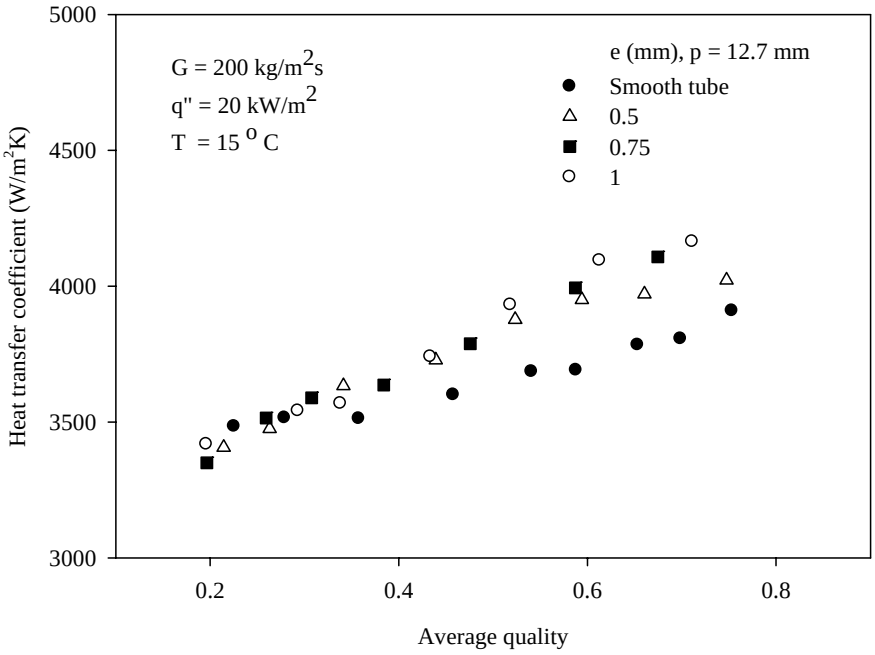

Figure 5.28 Effect of corrugation depth on evaporation heat transfer coefficient for G = 200 kg/m^{2}s, q" = 20 kW/m^2 and T = 15 °C.

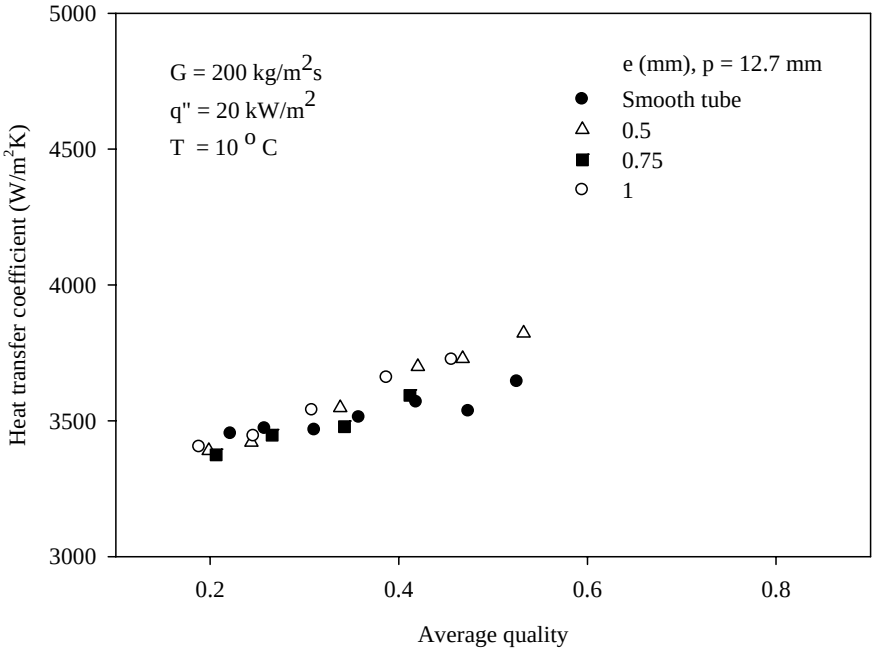

Figure 5.29 Effect of corrugation depth on evaporation heat transfer coefficient for G = 200 kg/m^{2}s, q" = 20 kW/m^2 and T = 10 °C.

5.1.2 Two-phase friction factor

The comparison of the experimental results for the smooth tube to those correlations proposed by Lockhart and Martinelli (1949) and Chisholm (1973) is displayed in Figure 5.30. The figure shows that more than 70% of the data measured from the present study fall within 20% of the proposed correlation.

5.1.2.1 Effect of mass flux

The effects of mass flux on the two-phase friction factor of evaporation are shown in Figs. 5.31-5.35. These graphs show the relationship between the two-phase friction factor and the equivalent Reynolds number at constant saturation temperature of evaporation and heat flux values for mass fluxes of 200, 300, and 400 kg/m^{2}s. These plots show that the two-phase friction factor decreases with increasing equivalent Reynolds number. There are two reasons for this. Firstly, the frictional pressure drop

increases with increasing vapor quality. This is because, at higher vapor quality, the higher velocity of vapor flow causes more shear stress at the interface of the vapor and liquid film. Moreover, the secondary flow that becomes stronger at higher vapor velocity will produce more entrainment and redeposition of droplets, causing more flow turbulence. Secondly, the equivalent Reynolds number increases with increasing vapor quality. This is because the increasing in average quality increases the equivalent mass flux, according to Eq. (4.18). As the equivalent mass flux increases, the equivalent Reynolds number also increases, according to Eq. (4.17). It can be seen that both frictional pressure drop and equivalent Reynolds number increase with an increase in average quality. According to Eq. (4.16), it is found that the equivalent Reynolds number dominates the two-phase friction factor. Therefore, the increase in average quality causes the two-phase friction factor to decrease. The results also indicate that the two-phase friction factor at higher mass flux is always higher than that at lower mass flux for a given equivalent Reynolds number. This is due to the fact that the increase of mass flux raises the two-phase velocity, which leads to higher intensity of secondary flow. Furthermore, the entrainment and redeposition of droplets are increased by secondary effects, causing more flow turbulence. Consequently, the shear stress at the interface of the vapor and liquid film increases. As a result, the pressure drop increases with the rise of mass flux.

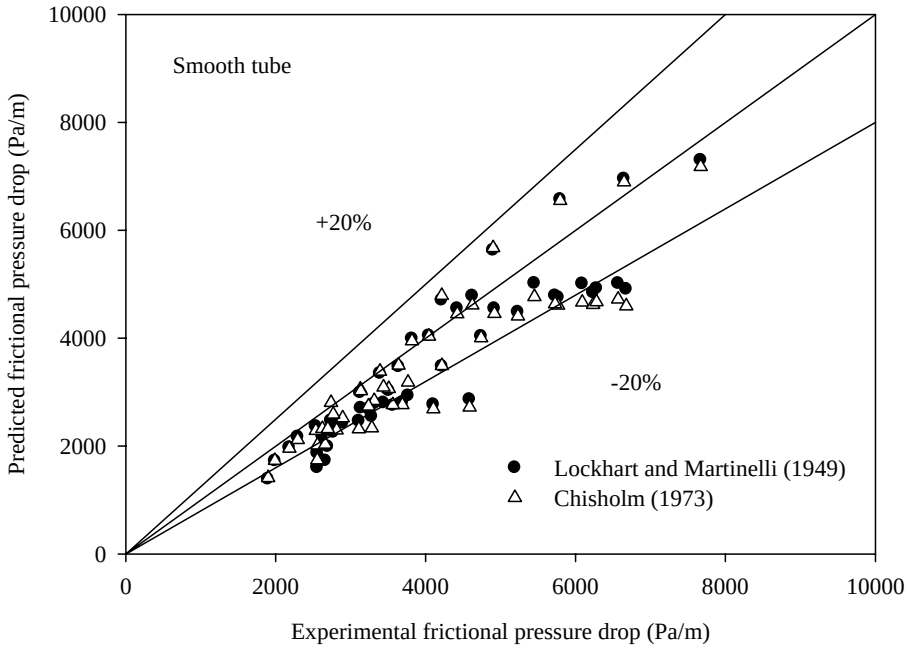

Figure 5.30 Comparison of experimental evaporation frictional pressure drop data with existing correlations.

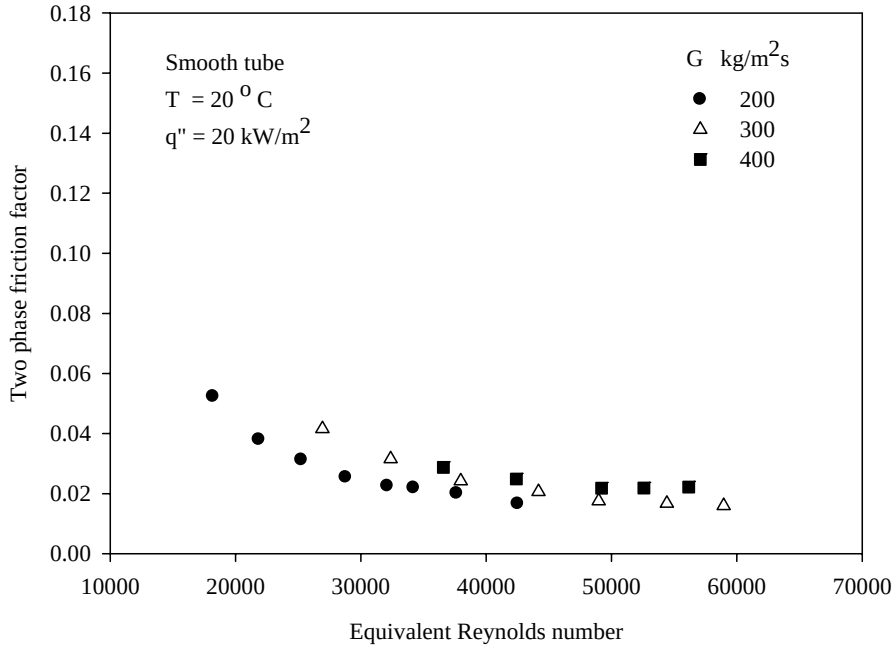

Figure 5.31 Effect of mass flux on evaporation two-phase friction factor for a smooth tube.

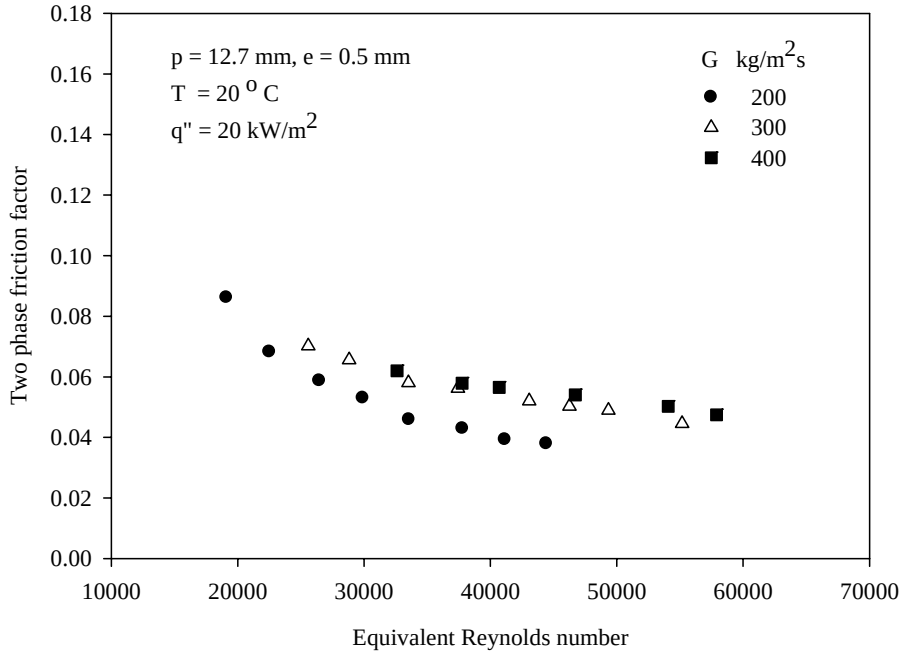

Figure 5.32 Effect of mass flux on evaporation two-phase friction factor for a tube with p = 12.7 mm and e = 0.5 mm.

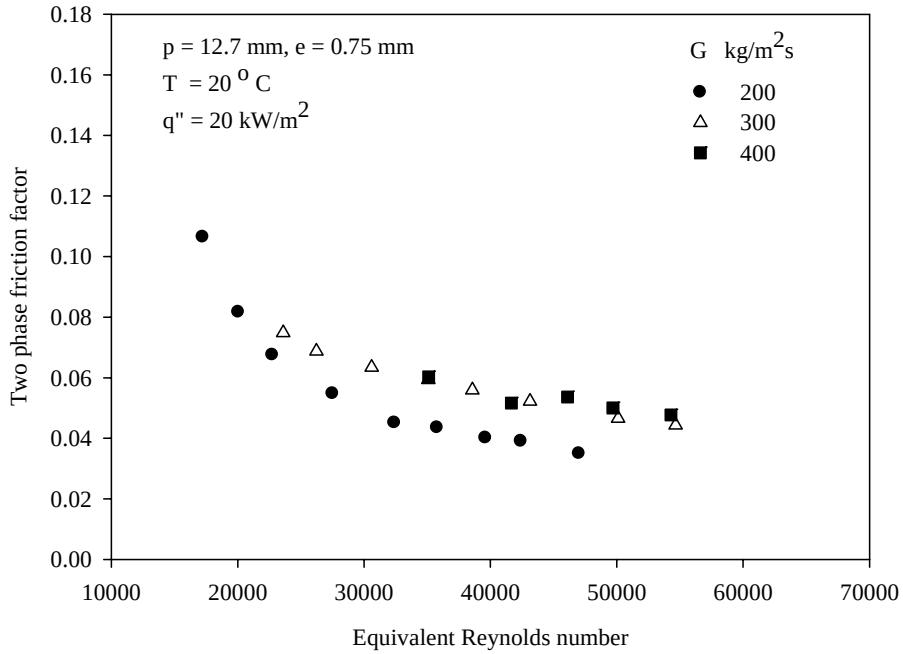

Figure 5.33 Effect of mass flux on evaporation two-phase friction factor for a tube with p = 12.7 mm and e = 0.75 mm.

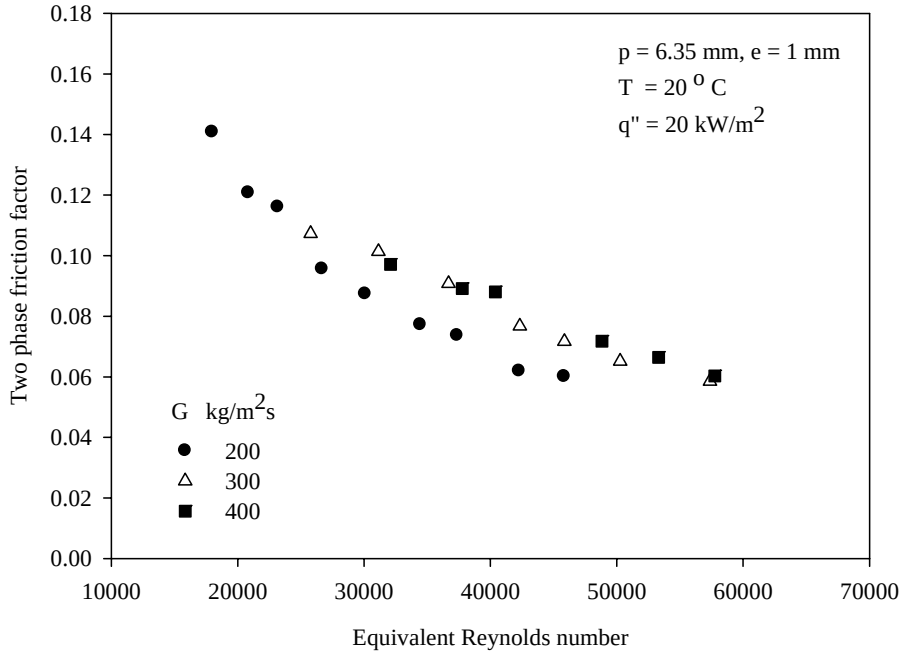

Figure 5.34 Effect of mass flux on evaporation two-phase friction factor for a tube with p = 6.35 mm and e = 1 mm.

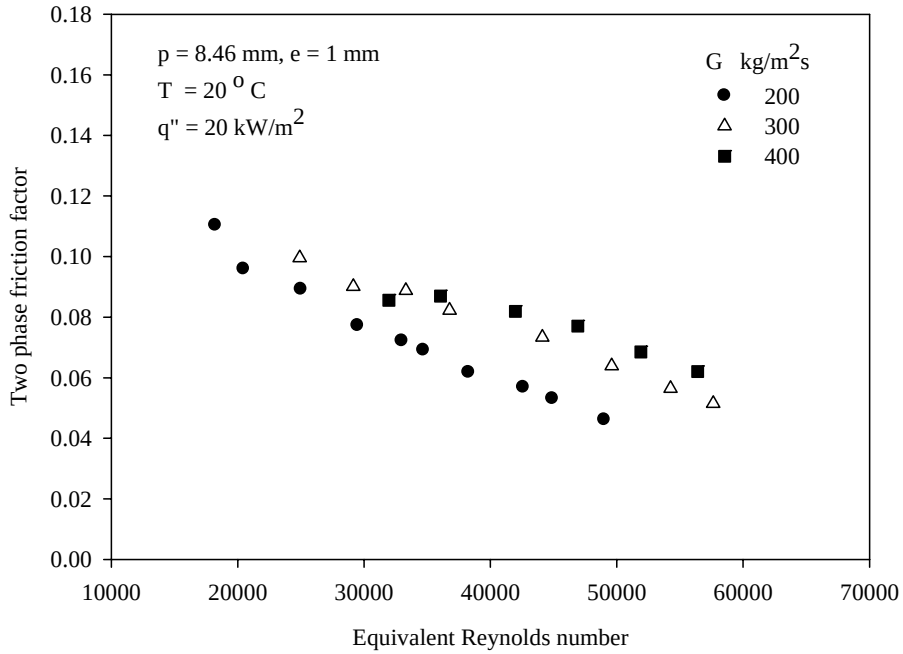

Figure 5.35 Effect of mass flux on evaporation two-phase friction factor for a tube with p = 8.46 mm and e = 1 mm.

5.1.2.2 Effect of heat flux

Figs. 5.36-5.39 present the variation of the two-phase friction factor with equivalent Reynolds number at a mass flux of 300 kg/m^2 s and a saturation temperature of 20 °C for heat fluxes of 20, 25 and 30 kW/m^2. These graphs show that the heat flux has an insignificant effect on the two-phase friction factor.

5.1.2.3 Effect of saturation temperature

Figs. 5.40-5.43 show the relationship between the two-phase friction factor and the equivalent Reynolds number at constant values of heat flux and mass flux for different saturation temperatures of 10, 15, and 20 °C. It is found that the saturation temperature has an unremarkable effect on the two-phase friction factor in the range of evaporating temperatures investigated.

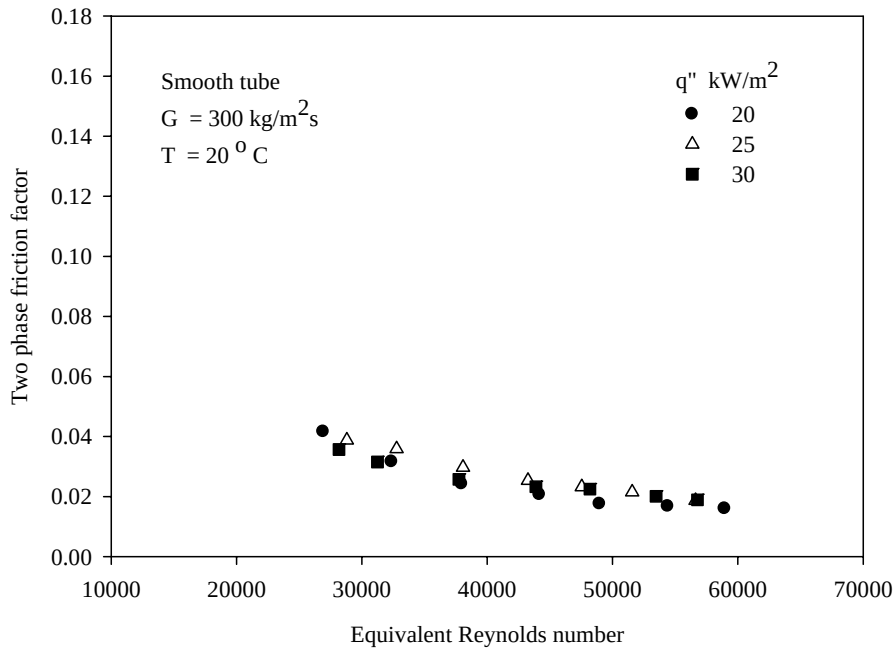

Figure 5.36 Effect of heat flux on evaporation two-phase friction factor for a smooth tube.

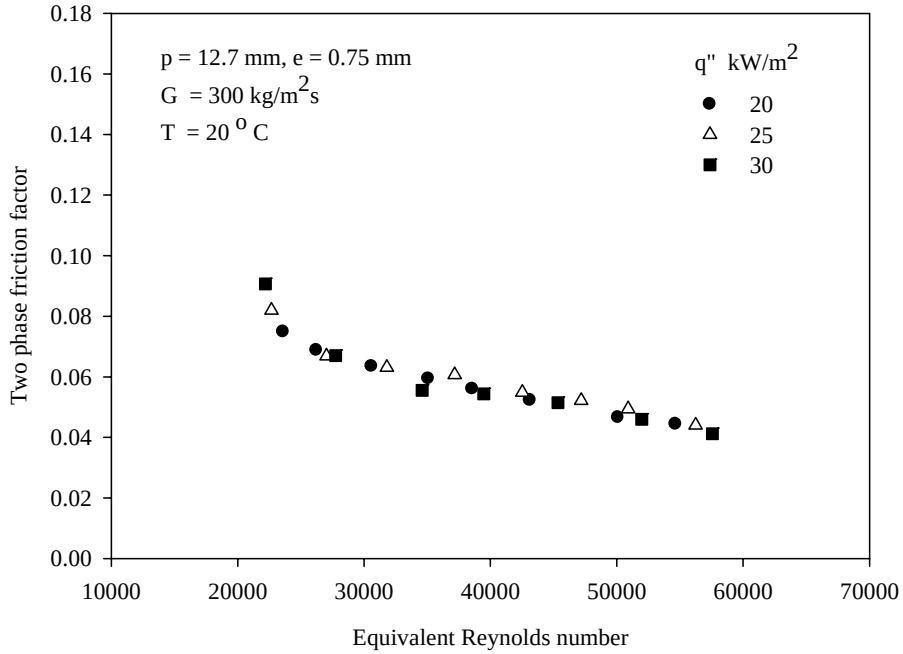

Figure 5.37 Effect of heat flux on evaporation two-phase friction factor for a tube with p = 12.7 mm and e = 0.75 mm.

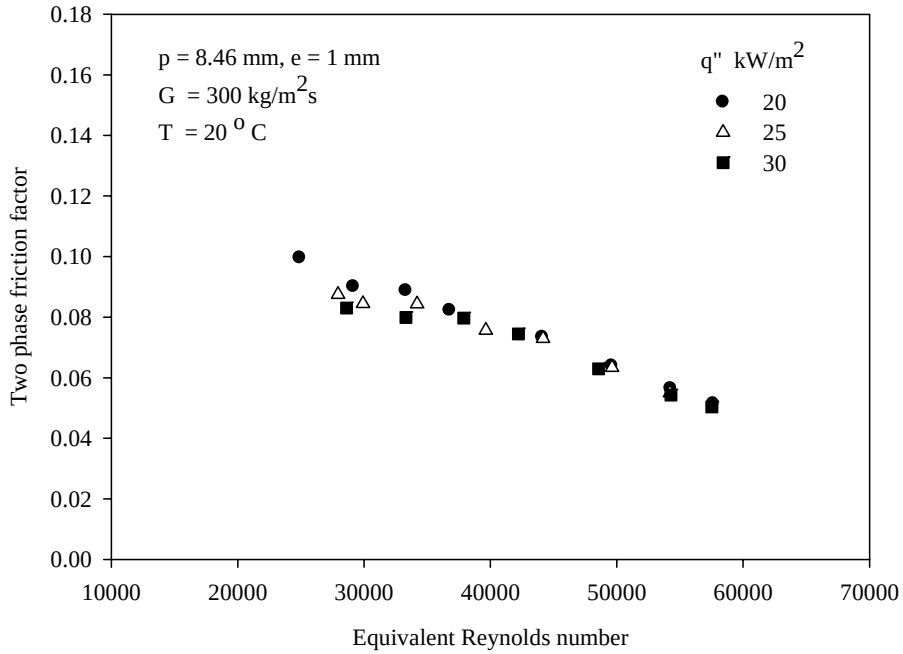

Figure 5.38 Effect of heat flux on evaporation two-phase friction factor for a tube with p = 8.46 mm and e = 1 mm.

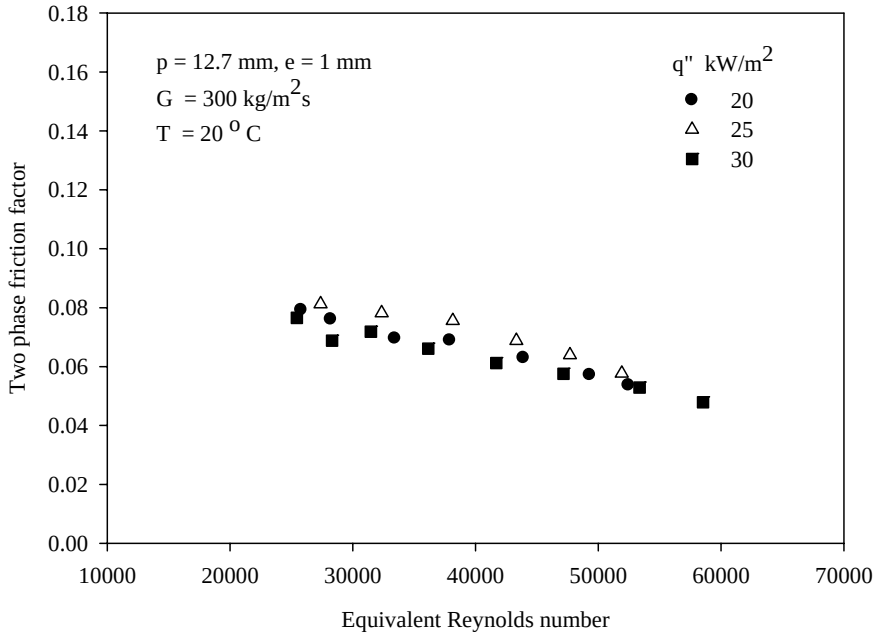

Figure 5.39 Effect of heat flux on evaporation two-phase friction factor for a tube with p = 12.7 mm and e = 1 mm.

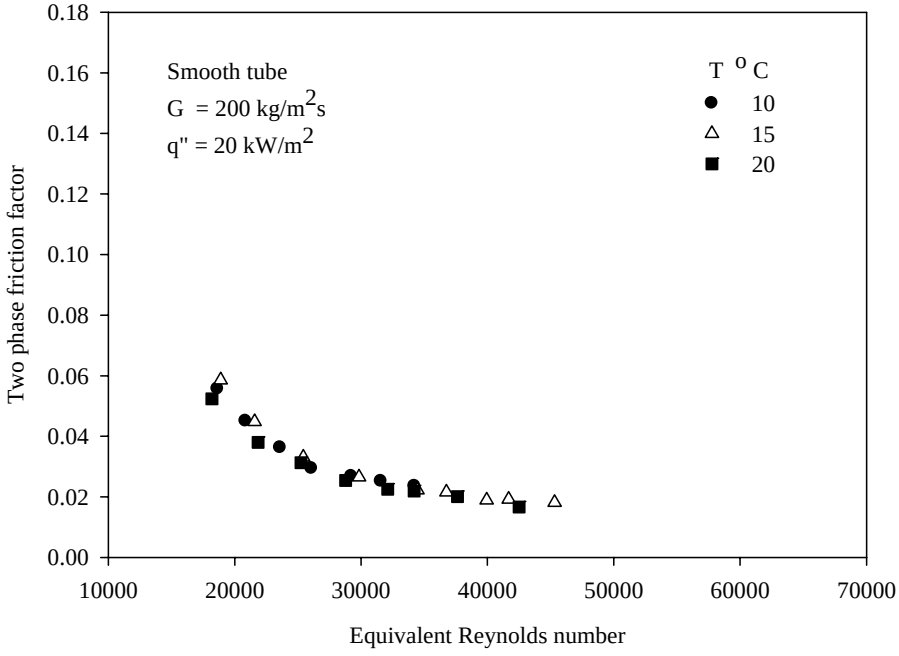

Figure 5.40 Effect of saturation temperature on evaporation two-phase friction factor for a smooth tube

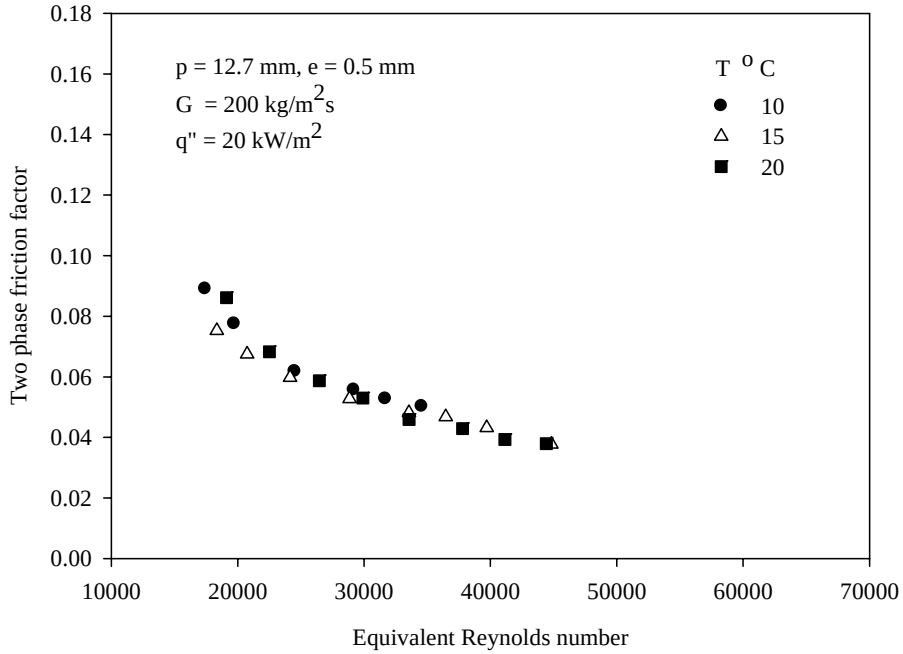

Figure 5.41 Effect of saturation temperature on evaporation two-phase friction factor for a tube with p = 12.7 mm and e = 0.5 mm.

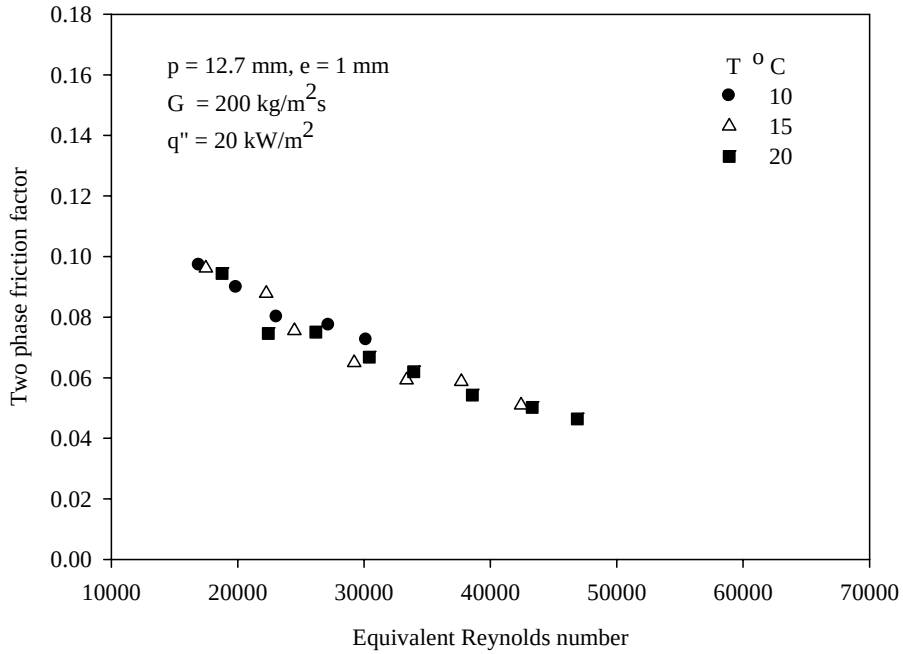

Figure 5.42 Effect of saturation temperature on evaporation two-phase friction factor for a tube with p = 12.7 mm and e = 1 mm.

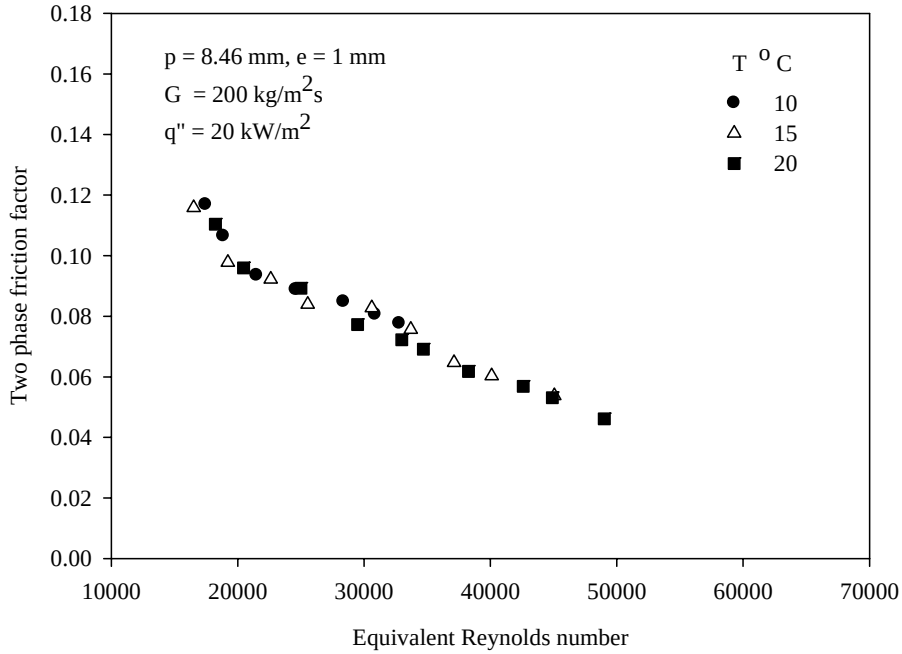

Figure 5.43 Effect of saturation temperature on evaporation two-phase friction factor for a tube with p = 8.46 mm and e = 1 mm.

5.1.2.4 The comparison between smooth and corrugated tubes

The variation of the two-phase friction factor with equivalent Reynolds number in smooth and corrugated tubes are illustrated in Figs. 5.44-5.55. It can be seen that the two-phase friction factor for the corrugated tubes is higher than that for the smooth tube. This is due to the pressure drop augmentation in corrugated tubes that is produced by (1) drag forces exerted on the flow field by the corrugation, (2) flow blockage due to area reduction, (3) turbulence augmentation, and (4) rotational flow produced by the corrugation (Vicente et al. 2004).

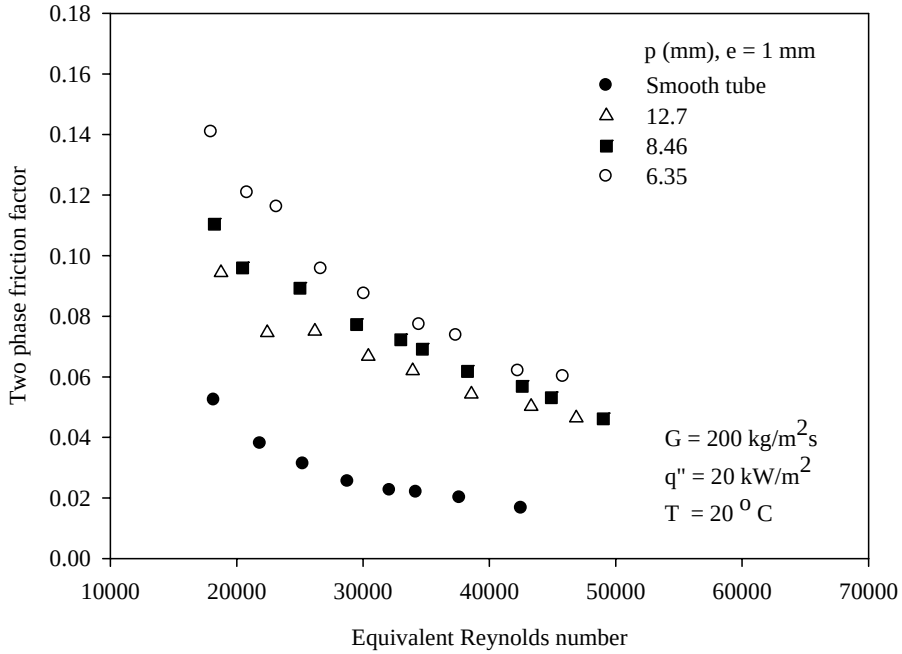

Figure 5.44 Effect of corrugation pitch on evaporation two-phase friction factor for G = 200 kg/m^{2}s, q" = 20 kW/m^2 and T = 20 °C.

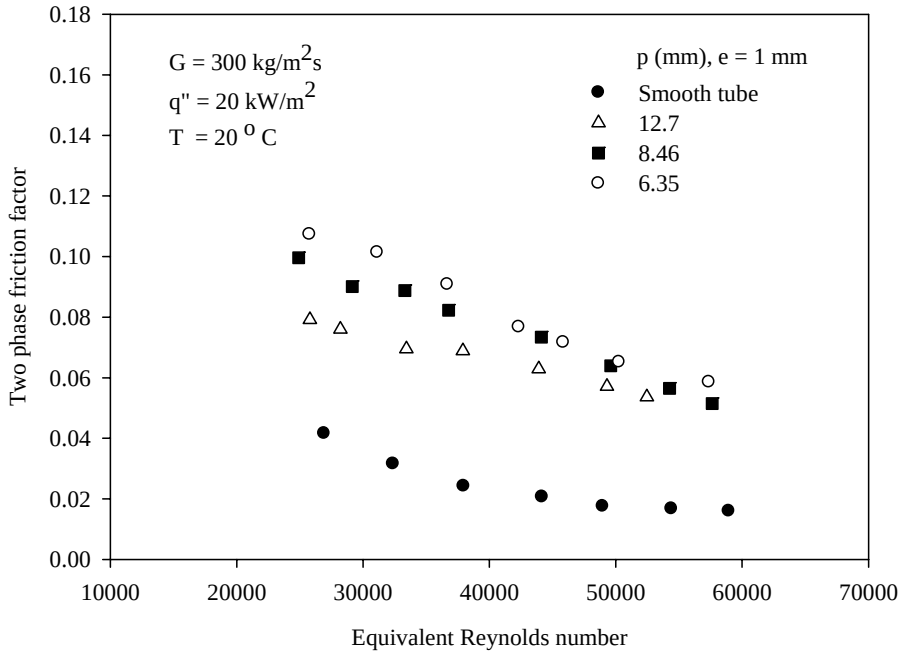

Figure 5.45 Effect of corrugation pitch on evaporation two-phase friction factor for G = 300 kg/m^{2}s, q" = 20 kW/m^2 and T = 20 °C.

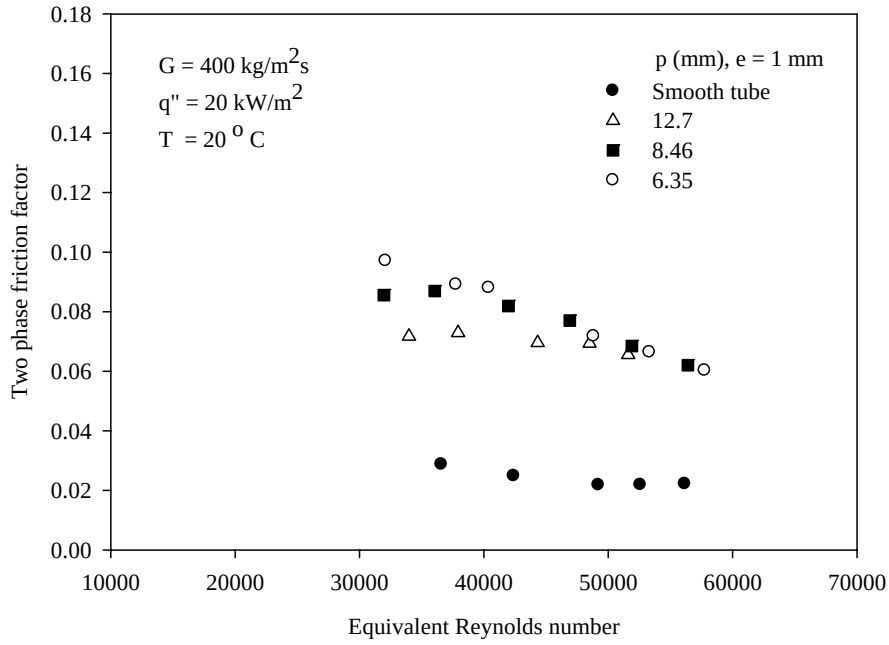

Figure 5.46 Effect of corrugation pitch on evaporation two-phase friction factor for G = 400 kg/m^{2}s, q" = 20 kW/m^2 and T = 20 °C.

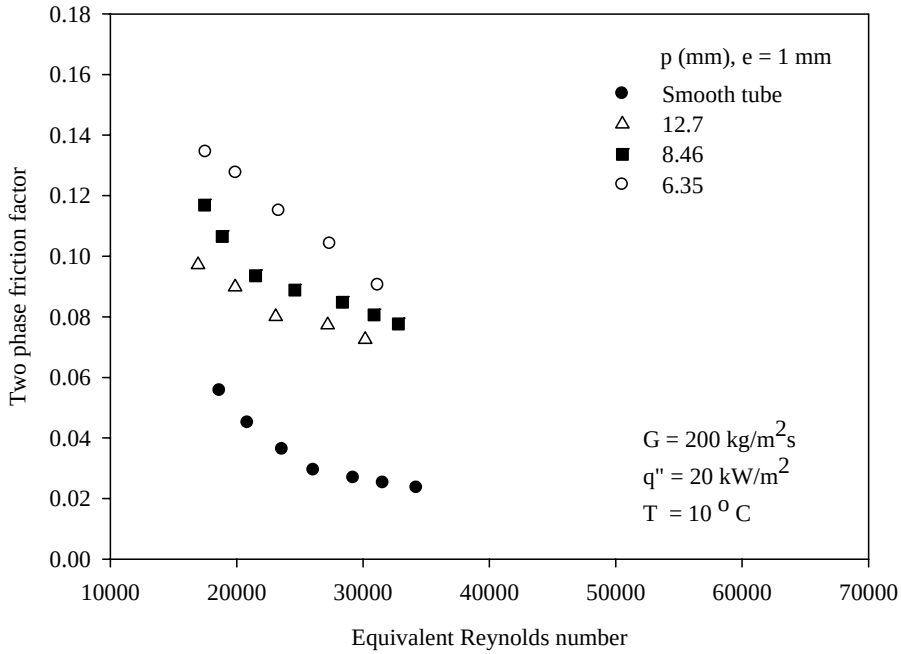

Figure 5.47 Effect of corrugation pitch on evaporation two-phase friction factor for G = 200 kg/m^{2}s, q" = 20 kW/m^2 and T = 10 °C.

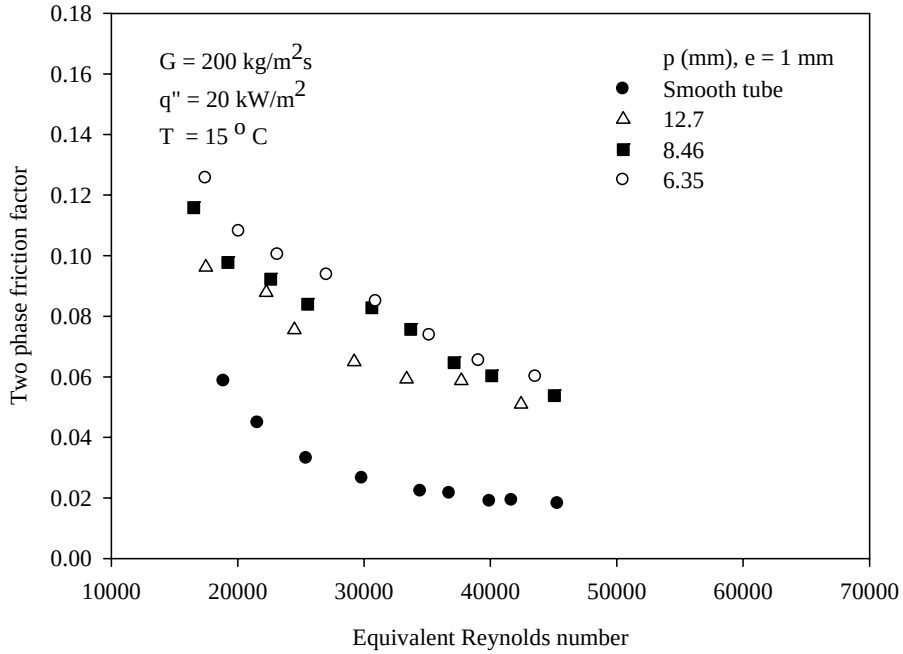

Figure 5.48 Effect of corrugation pitch on evaporation two-phase friction factor for G = 200 kg/m^{2}s, q" = 20 kW/m^2 and T = 15 °C.

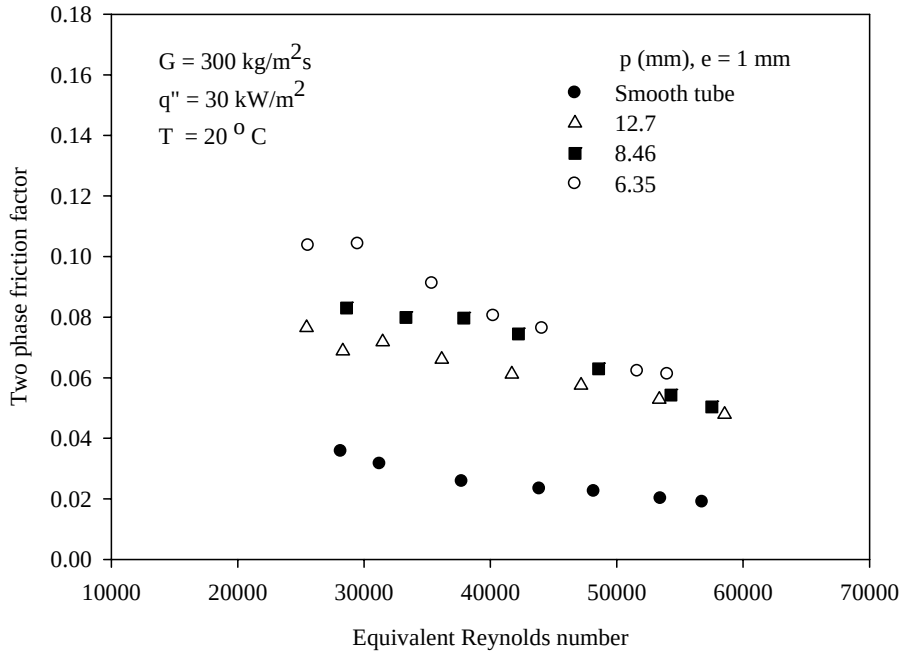

Figure 5.49 Effect of corrugation pitch on evaporation two-phase friction factor for G = 300 kg/m^{2}s, q" = 30 kW/m^2 and T = 20 °C.

Figs. 5.44-5.49 also show the effect of the corrugation pitch at constant corrugation depth of 1 mm on the two phase friction factor. The experimental results reveal that the higher two-phase friction factor is obtained from the tube with lower corrugation pitch. This is due to the fact that for lower corrugation pitch results in increased the corrugation surface, more turbulence of the fluid flow, and more pressure loss. The maximum value of two-phase friction factor enhancement corresponds to the tube with the lowest corrugation pitch of 6.35 mm. This tube increases the two-phase friction factor by 280% in comparison with the smooth tube at the mass flux of 200 kg/m^2s, heat flux of 20 kW/m^2 and saturation temperature of 20 °C.

Figs. 5.50-5.55 illustrate the effect of the tube having different corrugation depth and a constant corrugation pitch of 12.7 mm on the two-phase friction factor. From these figures, it can be seen that the tube having a corrugation depth of 1 mm has higher two-phase friction factor than that obtained from the tube having corrugation depth of 0.75 mm and 0.5 mm. The maximum value of two-phase friction factor enhancement is up to 220% for a depth of 1 mm in comparison with the smooth tube. For the tube having corrugation depths of 0.75 mm and 0.5 mm, the two-phase friction factor obtained from those tubes are nearly the same. These tubes increase the two-phase friction factor up to 160% in comparison with the smooth tube.

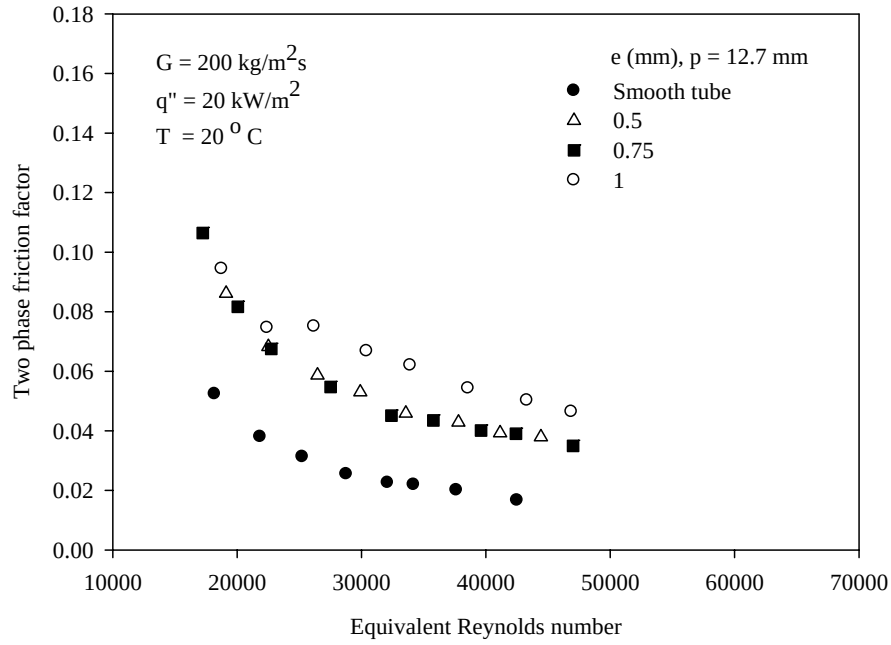

Figure 5.50 Effect of corrugation depth on evaporation two-phase friction factor for G = 200 kg/m^{2}s, q" = 20 kW/m^2 and T = 20 °C.

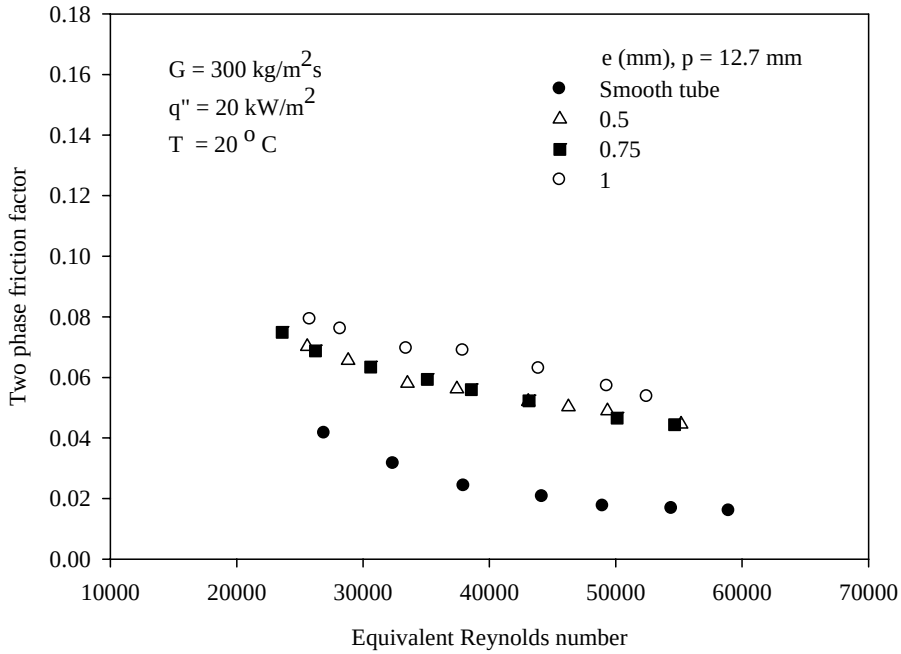

Figure 5.51 Effect of corrugation depth on evaporation two-phase friction factor for G = 300 kg/m^{2}s, q" = 20 kW/m^2 and T = 20 °C.

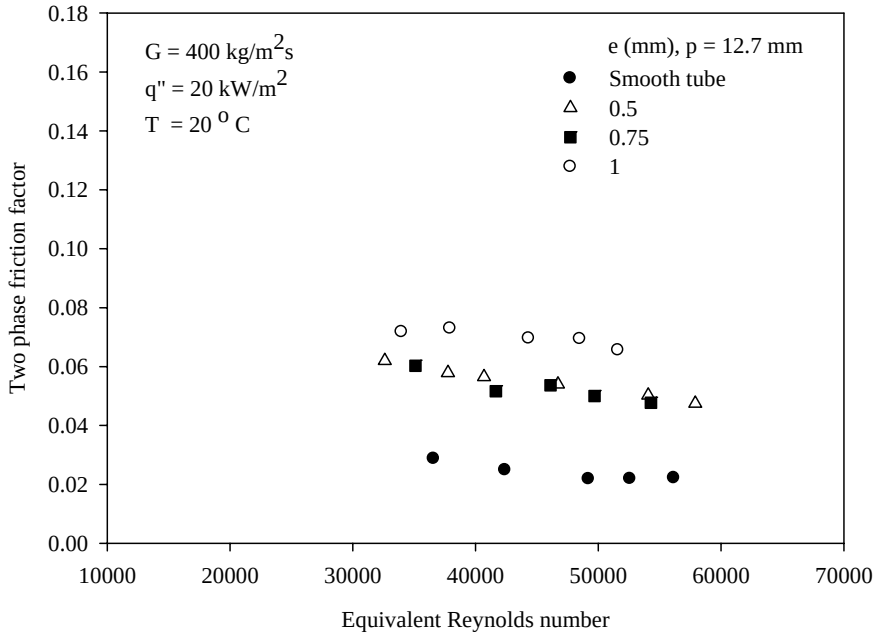

Figure 5.52 Effect of corrugation depth on evaporation two-phase friction factor for G = 400 kg/m^{2}s, q" = 20 kW/m^2 and T = 20 °C.

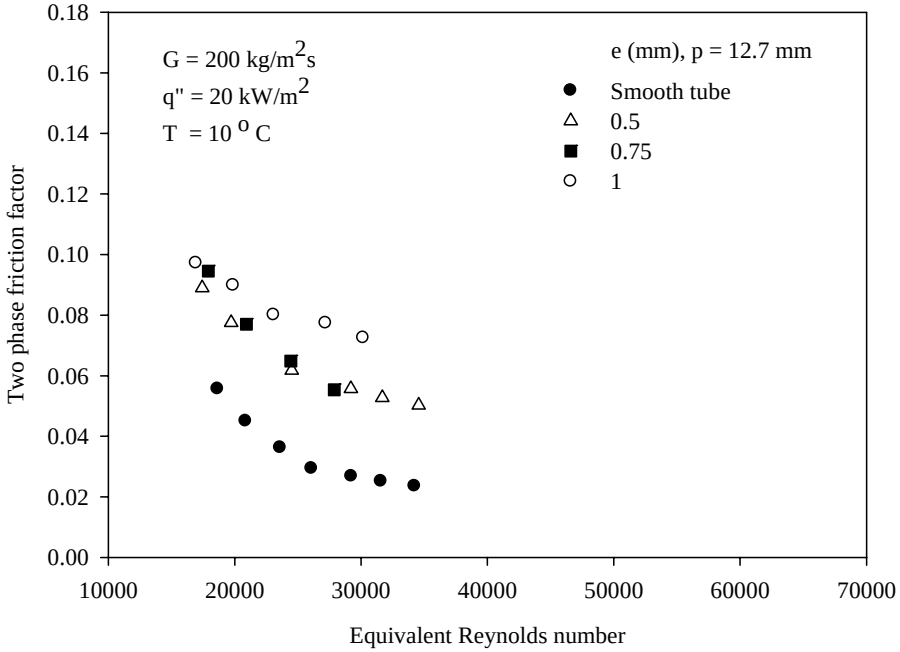

Figure 5.53 Effect of corrugation depth on evaporation two-phase friction factor for G = 200 kg/m^{2}s, q" = 20 kW/m^2 and T = 10 °C.

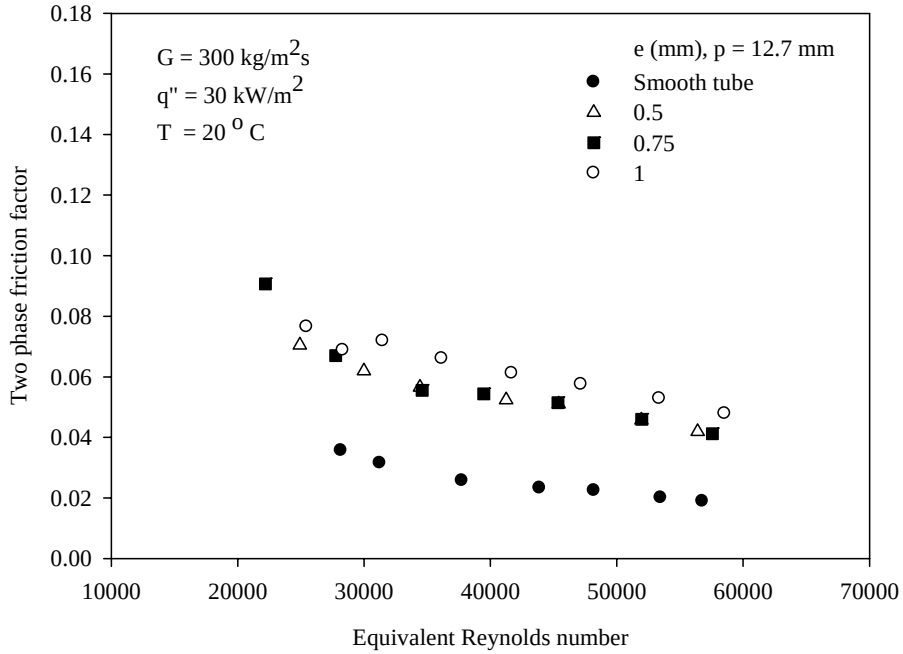

Figure 5.54 Effect of corrugation depth on evaporation two-phase friction factor for G = 300 kg/m^{2}s, q" = 30 kW/m^2 and T = 20 °C.

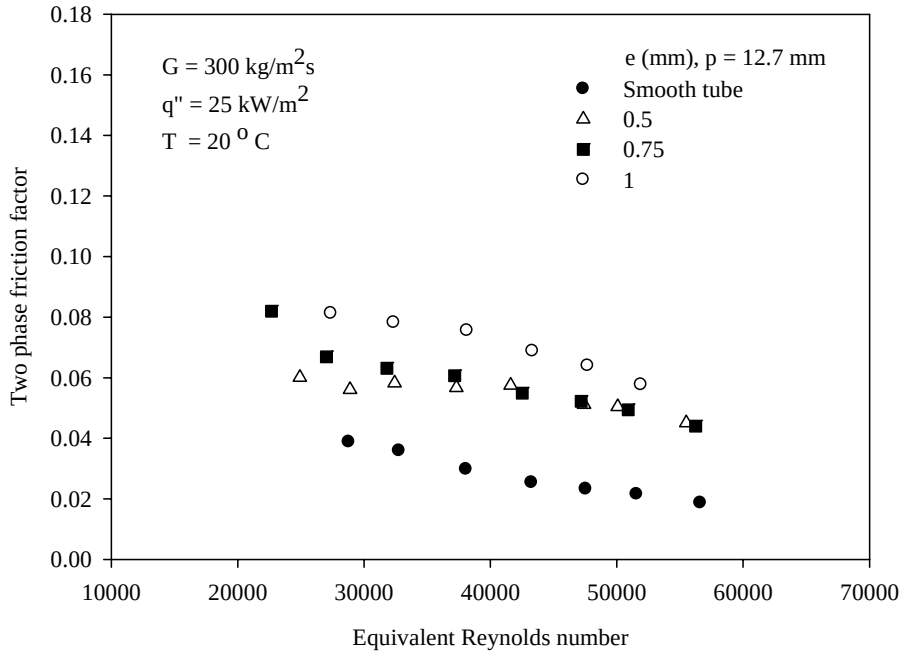

Figure 5.55 Effect of corrugation depth on evaporation two-phase friction factor for G = 300 kg/m^{2}s, q" = 25 kW/m^2 and T = 20 °C.

5.2 Heat transfer and flow characteristics of HFC-134a during condensation inside vertical corrugated tube.

Data are presented in the forms of average heat transfer coefficient and frictional pressure drop. The effects of mass flux, heat flux, and condensing temperature on the average heat transfer coefficient and frictional pressure drop are investigated.

5.2.1 Average heat transfer coefficient

As demonstrated in Fig. 5.56, the average heat transfer coefficient is compared with established correlations proposed by Traviss et al. (1972), Cavallini and Zecchin (1974), Shah (1979) and Dobson and Chato (1998). It is found that these correlations can describe almost all of the heat transfer coefficients to within 30%.

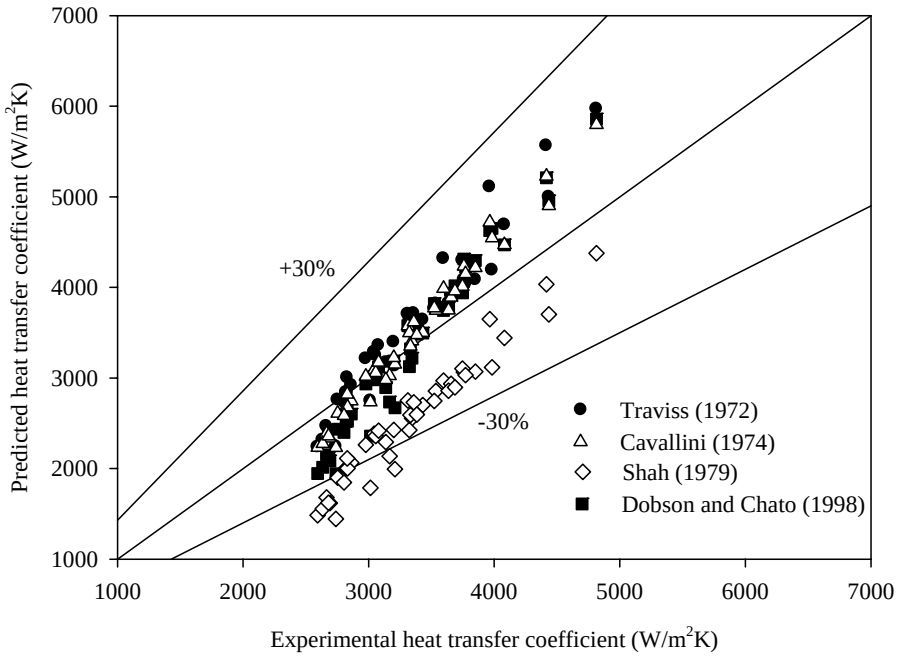

Figure 5.56 Comparison of experimental condensation heat transfer coefficient data with existing correlations.

5.2.1.1 Effect of mass flux

In Figs. 5.57 and 5.58, the variation of the average heat transfer coefficient with average vapor quality at fixed saturation temperature and heat flux values and different mass fluxes of 300, 400, and 500 kg/m^{2}s is shown. The quality shown in the present work is averaged from the inlet quality and outlet quality of the test section. It can be observed that higher average vapor quality results in higher average heat transfer coefficient. This is because at high vapor quality, the velocity of the vapor flow is high, resulting in high shear stress at the interface between the vapor and liquid film. The increasing shear stress causes more entrainment of droplets, which makes the liquid film thinner. As a result, the thermal resistance is decreased. These figures also show the effect of mass flux on the average heat transfer coefficient. It is found that for a given vapor quality, the average heat transfer coefficient is increased with the mass flux. This is because the increase in the mass flux also increases the velocity of the vapor and liquid film and the flow turbulence as a result of enhancing convective heat transfer.

5.2.1.2 Effect of heat flux

The effect of the heat flux on the average heat transfer coefficient can be seen from Figs. 5.59 and 5.60. They show the variation of the average heat transfer coefficient as a function of average quality at fixed saturation temperature and mass flux values with different values of heat flux: 20, 25, and 30 kW/m^2. The experimental data reveal that the heat flux has slight effects on the average heat transfer coefficient.

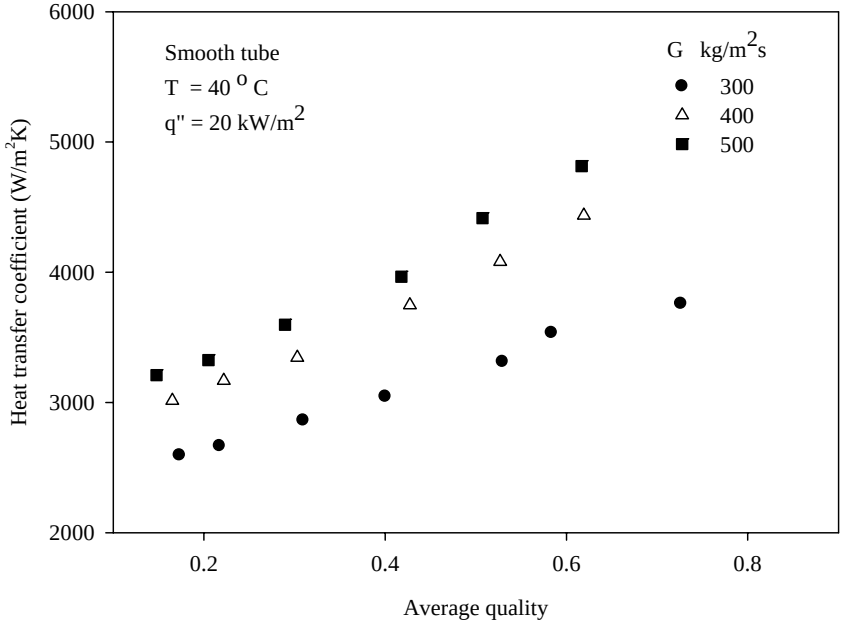

Figure 5.57 Effect of mass flux on condensation heat transfer coefficient for a smooth tube.

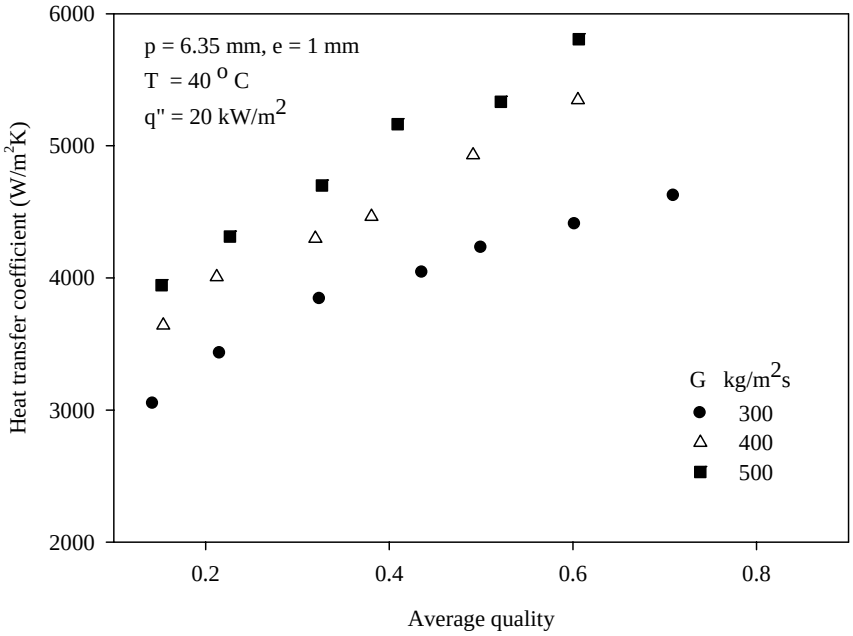

Figure 5.58 Effect of mass flux on condensation heat transfer coefficient for a tube with p = 6.35 mm and e = 1 mm.

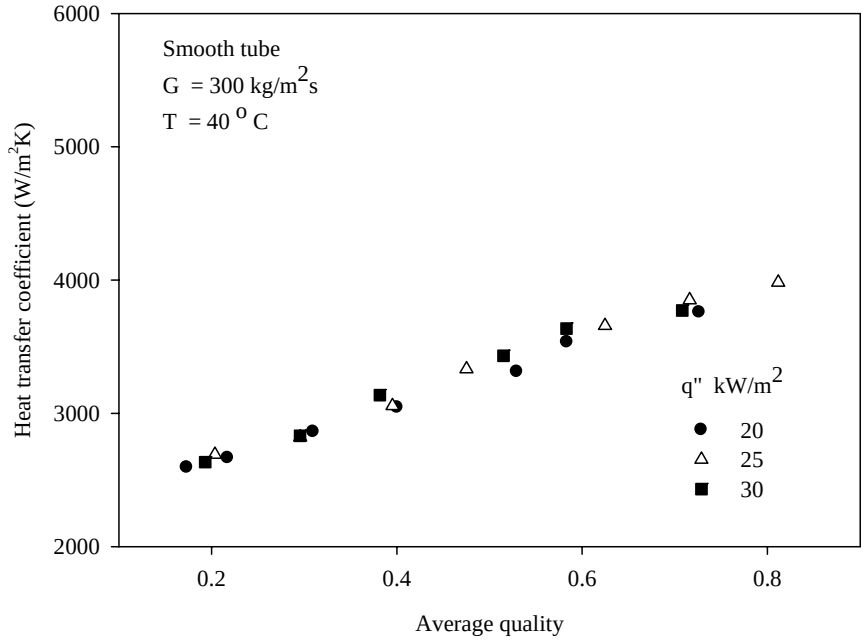

Figure 5.59 Effect of heat flux on condensation heat transfer coefficient for a smooth tube.

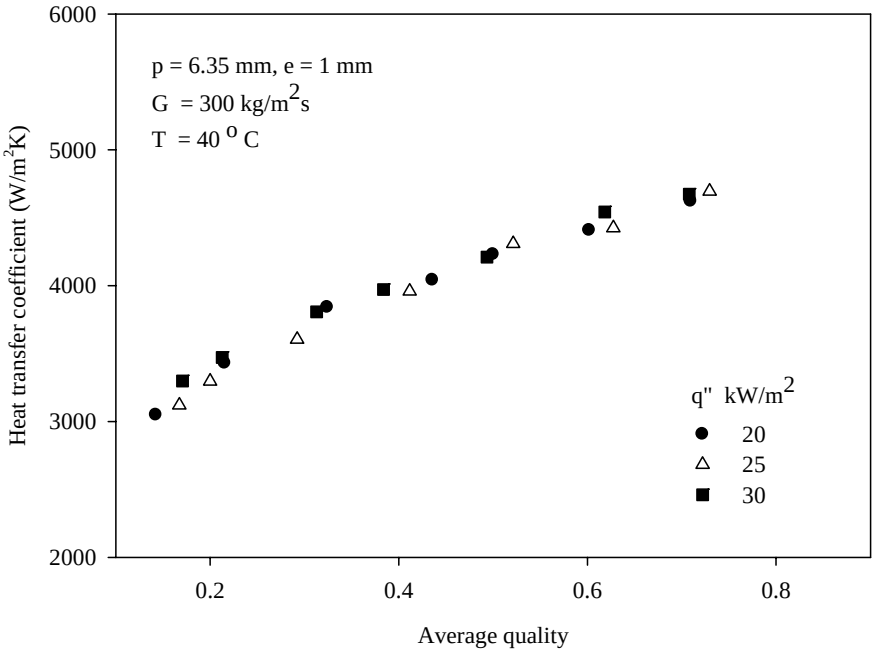

Figure 5.60 Effect of heat flux on condensation heat transfer coefficient for a tube with p = 6.35 mm and e = 1 mm.

5.2.1.3 Effect of saturation temperature

In order to study the effect of saturation temperature on the average heat transfer coefficient, three different saturation temperature values of 40, 45, and 50 °C are used in the experiment. Experimental results are displayed in Figs. 5.61 and 5.62. These figures present the variation in the average heat transfer coefficient with the average quality at constant mass flux and heat flux. It is found that the heat transfer coefficient is changed by a relatively small amount with increasing condensing temperature.

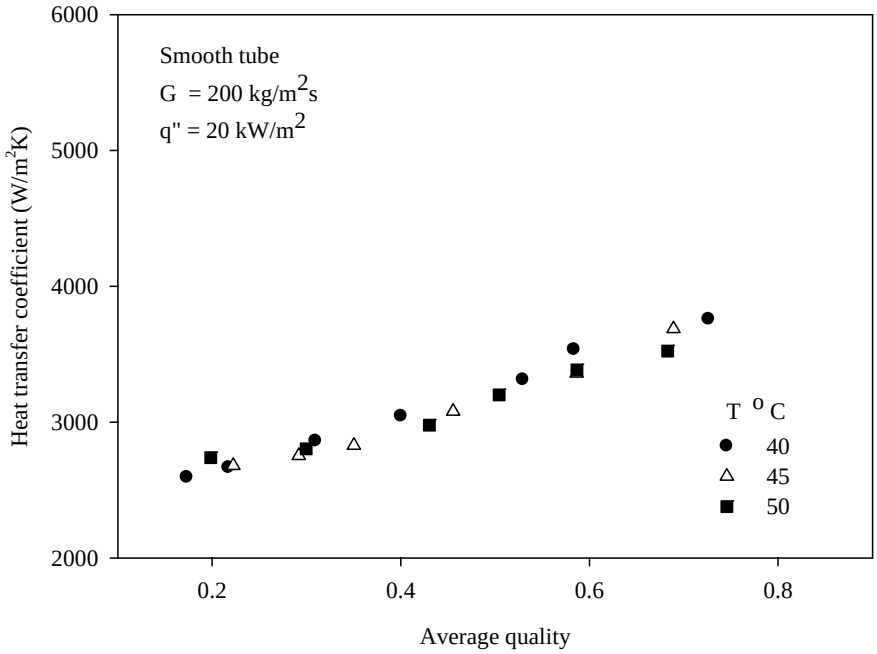

Figure 5.61 Effect of saturation temperature on condensation heat transfer coefficient for a smooth tube.

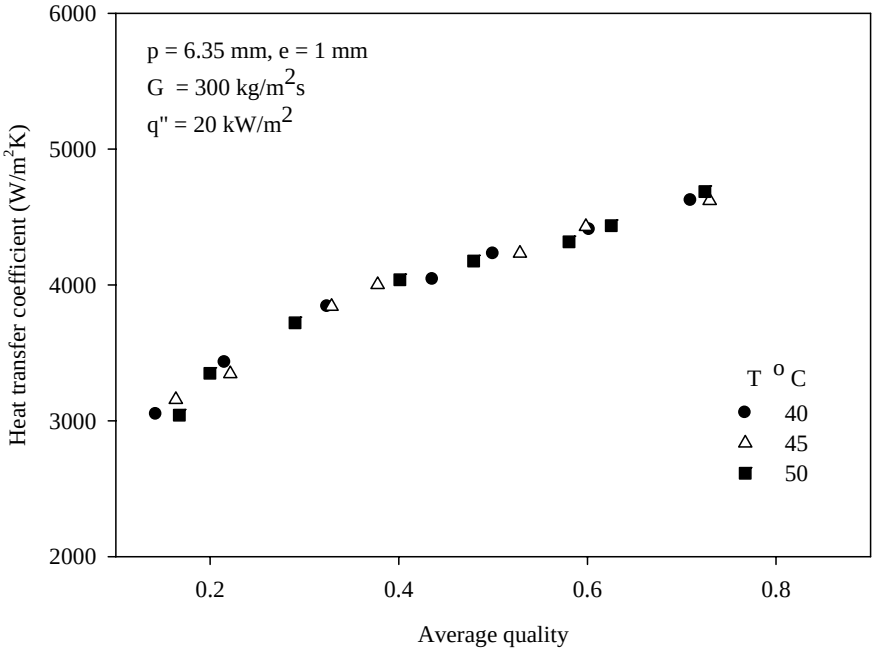

Figure 5.62 Effect of saturation temperature on condensation heat transfer coefficient for a tube with p = 6.35 mm and e = 1 mm.

5.2.1.4 The comparison between smooth and corrugated tubes

The comparisons of the condensing heat transfer coefficient in the smooth and the corrugated tubes are displayed in Figs. 5.63-5.68. The results show that the heat transfer coefficient for the corrugated tubes is higher than that for the smooth tube. This is due to the fact that the corrugated surface promotes more turbulence by increasing the mixing of the refrigerant flow. The corrugated tube not only generates more turbulence than the smooth tube but also increases the heat transfer area. The corrugated tubes may provide periodic redevelopment of the boundary layers, causing more effective heat transfer. In other words, the thermal boundary layers inside the corrugated tubes are thinner than those inside the smooth tube (Bilen et al. 2009).

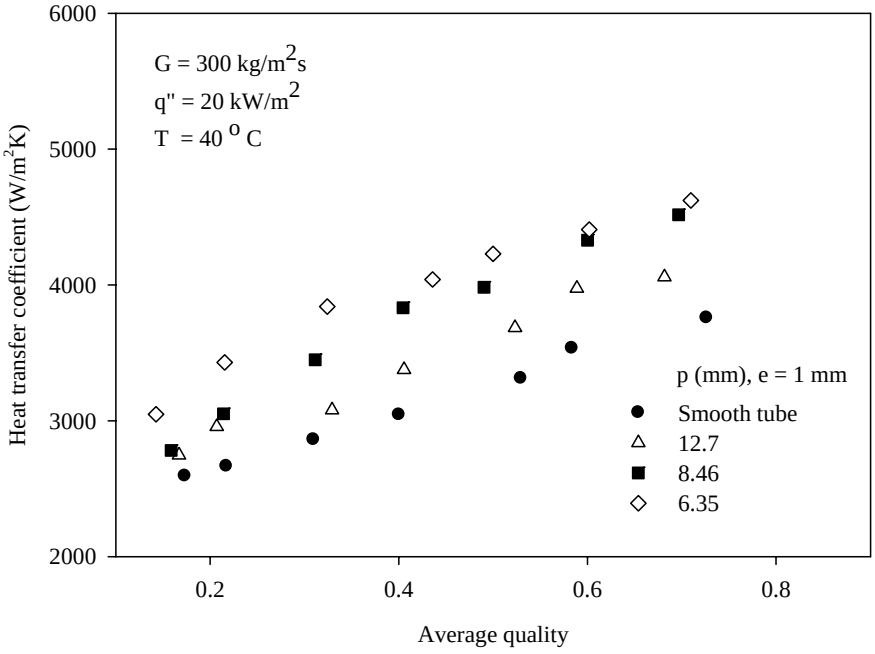

Figure 5.63 Effect of corrugation pitch on condensation heat transfer coefficient for G = 300 kg/m^{2}s, q" = 20 kW/m^2 and T = 40 °C.

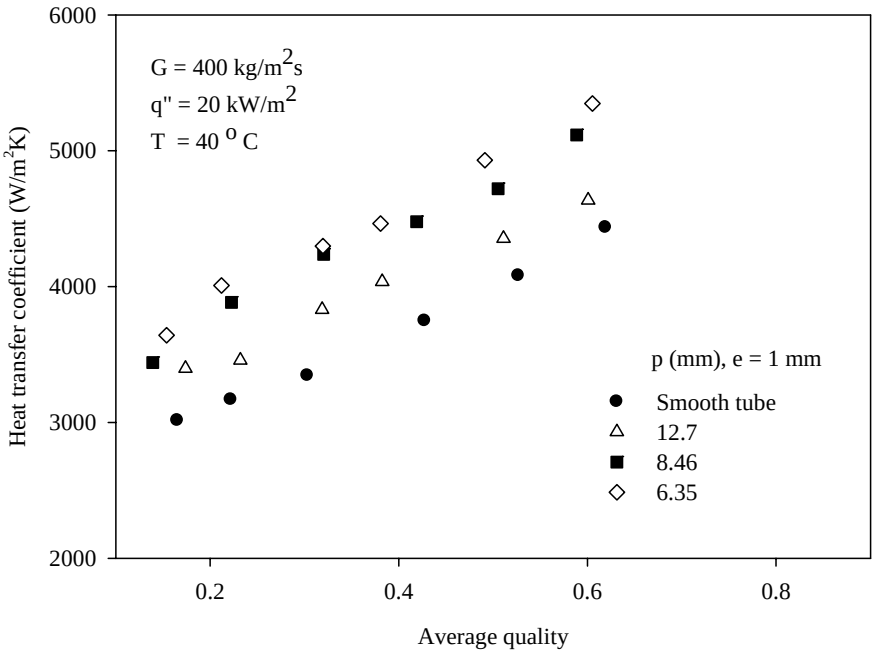

Figure 5.64 Effect of corrugation pitch on condensation heat transfer coefficient for G = 400 kg/m^{2}s, q" = 20 kW/m^2 and T = 40 °C.

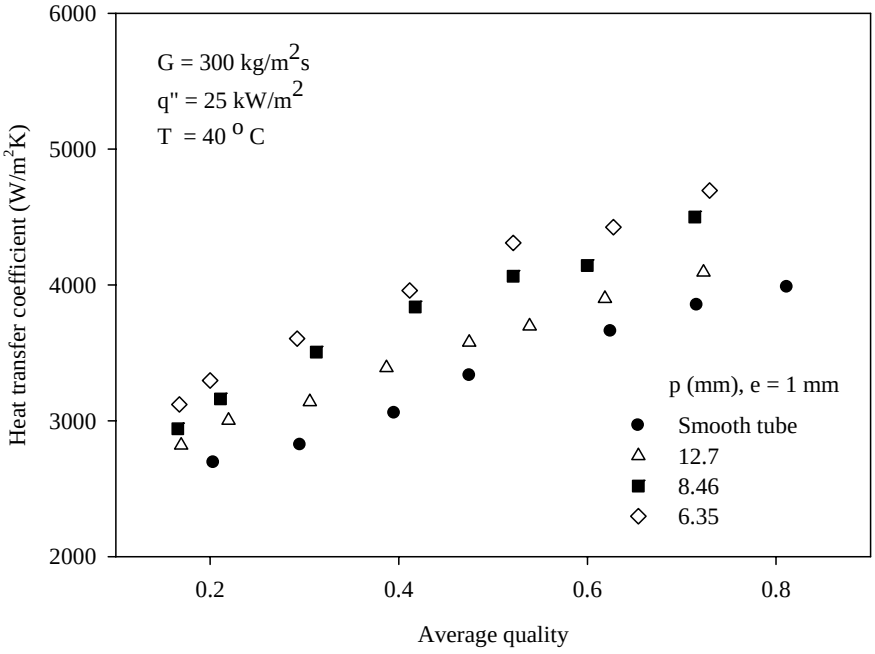

Figure 5.65 Effect of corrugation pitch on condensation heat transfer coefficient for G = 300 kg/m^{2}s, q" = 25 kW/m^2 and T = 40 °C.

Figs. 5.63-5.65 also show the variation of the average heat transfer coefficient with average vapor quality in the smooth tube and corrugated tube having different corrugation pitches of 6.35, 8.46 and 12.7 mm. It can be seen that the increase in the heat transfer augmentation for the tube with lower corrugation pitch is due to more mixing of the fluid flow and heat transfer area. Maximum heat transfer enhancement is up to 28% for the tube having corrugation pitch of 6.35 mm in comparison with the smooth tube.

Figs. 5.66-5.68 demonstrate the effect of the corrugation depth on the heat transfer coefficient. The figures indicate that the corrugation depth has only small effect on the heat transfer coefficient. The maximum heat transfer coefficient of the corrugated tube is up to 12% higher than that for the smooth tube.

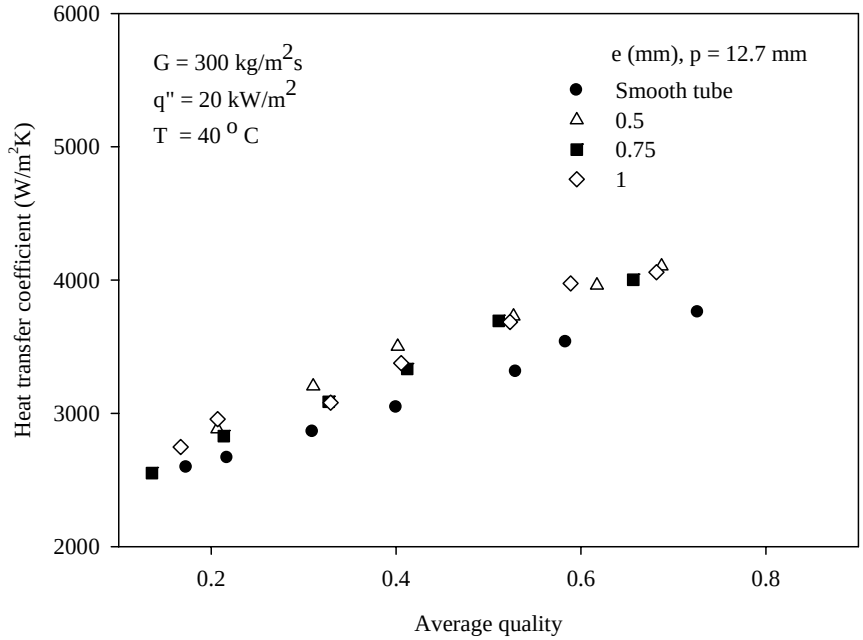

Figure 5.66 Effect of corrugation depth on condensation heat transfer coefficient for G = 300 kg/m^{2}s, q" = 20 kW/m^2 and T = 40 °C.

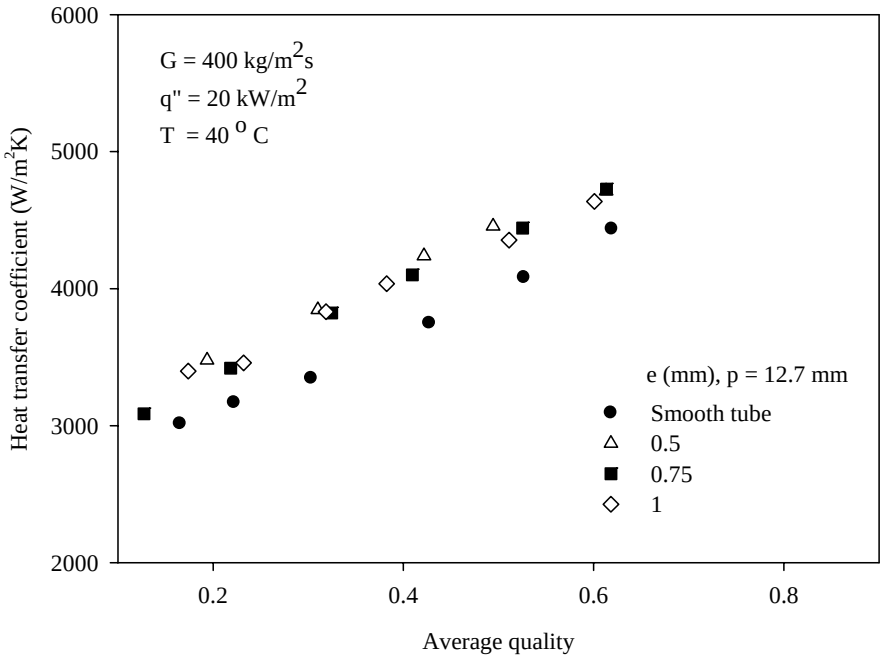

Figure 5.67 Effect of corrugation depth on condensation heat transfer coefficient for G = 400 kg/m^{2}s, q" = 20 kW/m^2 and T = 40 °C.

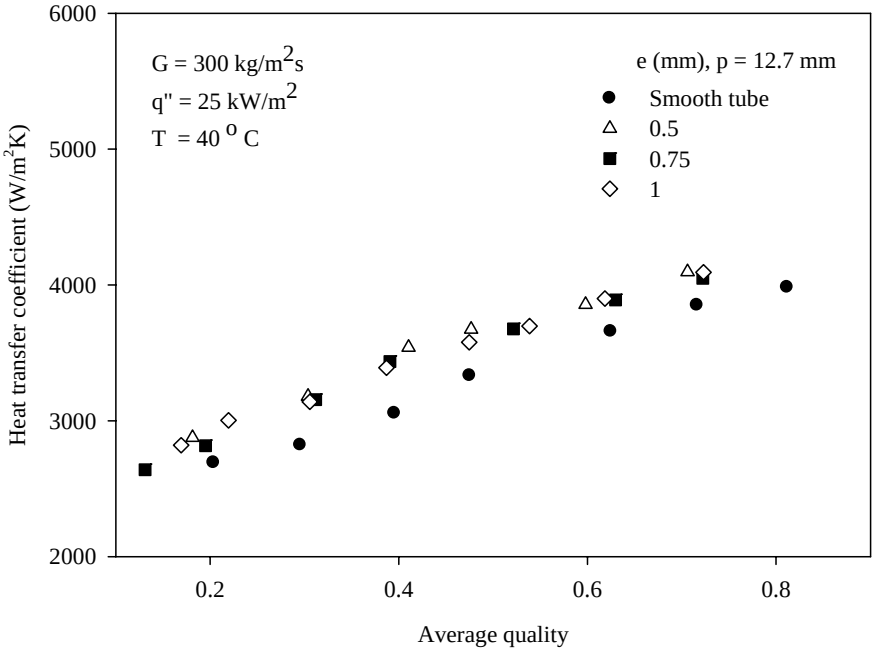

Figure 5.68 Effect of corrugation depth on condensation heat transfer coefficient for G = 300 kg/m^{2}s, q" = 25 kW/m^2 and T = 40 °C.

5.2.2 Frictional pressure drop

5.2.2.1 Effect of mass flux

Figs. 5.69 and 5.70 show the relationship between the frictional pressure drop and average quality, at constant condensing temperature and heat flux values, with varying mass fluxes of 300, 400 and 500 kg/m^{2}s. These plot show that the frictional pressure drop is increased with the rise of average vapor quality. This is because, as the vapor quality inside the tube is raised, the fluid velocity increases, which causes more shear stress at the interface between the vapor and liquid film. Moreover, the secondary flow that becomes stronger at higher vapor velocity will produce more entrainment and redeposition of droplets, causing more flow turbulence. In addition, it is observed that at equal vapor quality, the frictional pressure drop is increased with mass flux. This is due to the fact that the increase in mass flux will increase the vapor velocity and the flow

turbulence. For this reason, the shear stress at the interface of the vapor and liquid film increases and, as a result, the pressure drop is increased.

5.2.2.2 Effect of heat flux

Figs. 5.71 and 5.72 present the variation of the frictional pressure drop with average vapor quality at a mass flux of 300 kg/m^2 s and a saturation temperature of 40 °C for heat fluxes of 20, 25 and 30 kW/m^2. These graphs show that the heat flux has an insignificant effect on the frictional pressure drop in the range of investigated heat flux.

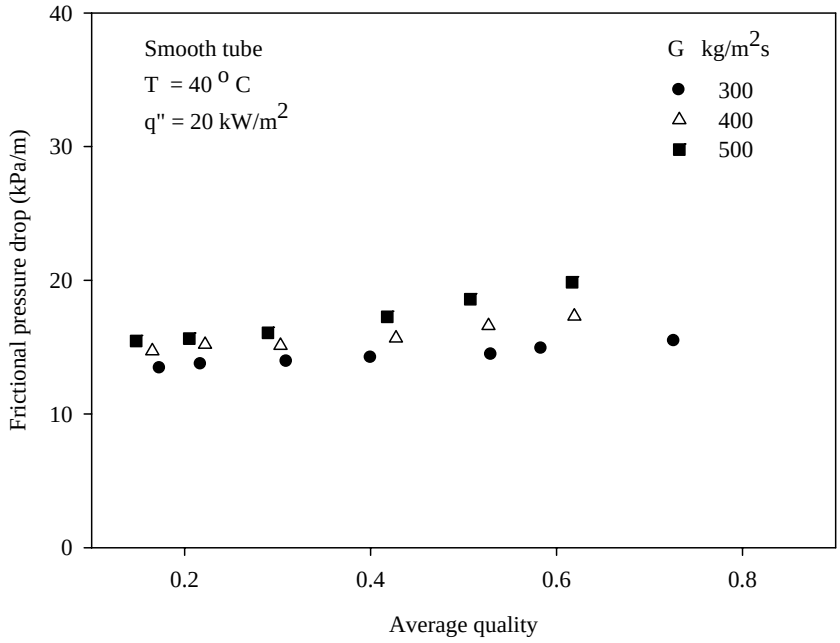

Figure 5.69 Effect of mass flux on condensation frictional pressure drop for a smooth tube.

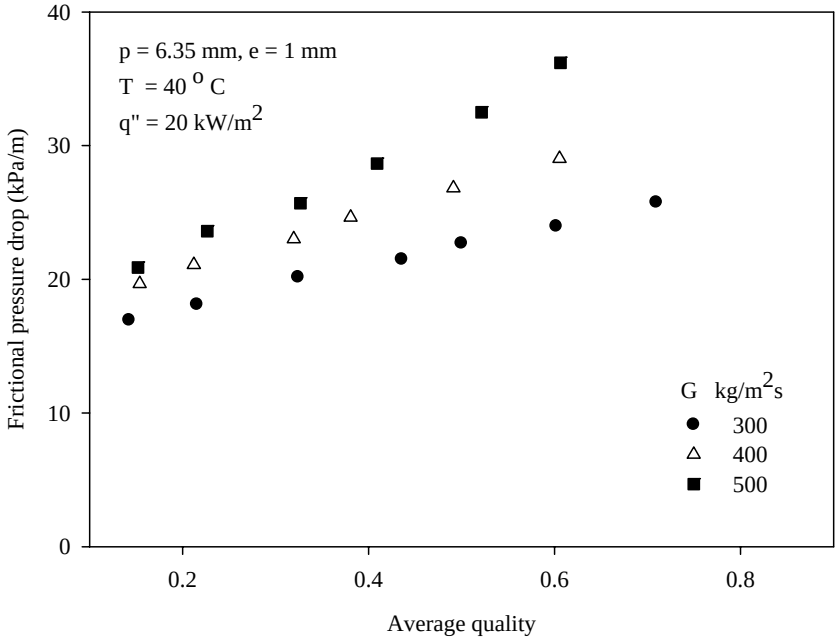

Figure 5.70 Effect of mass flux on condensation frictional pressure drop for a tube with p = 6.35 mm and e = 1 mm.

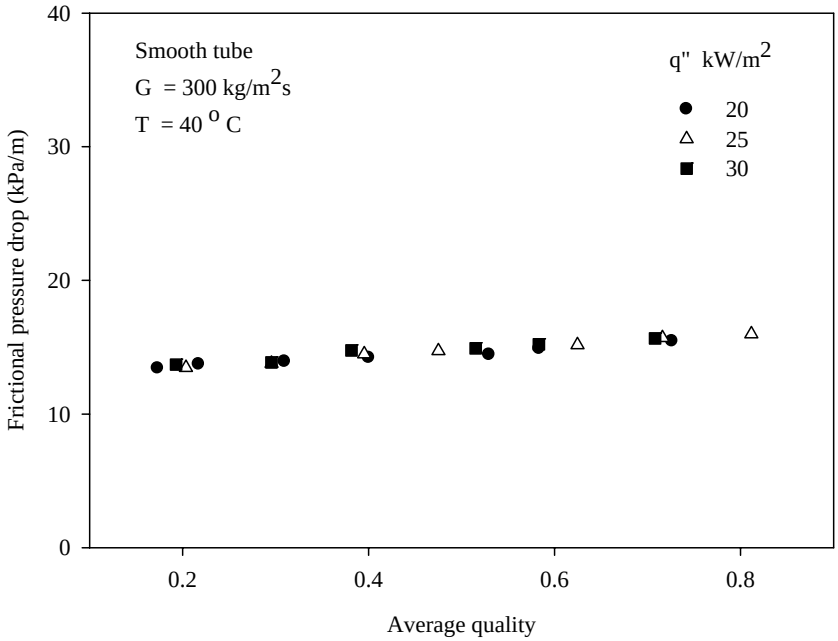

Figure 5.71 Effect of heat flux on condensation frictional pressure drop for a smooth tube.

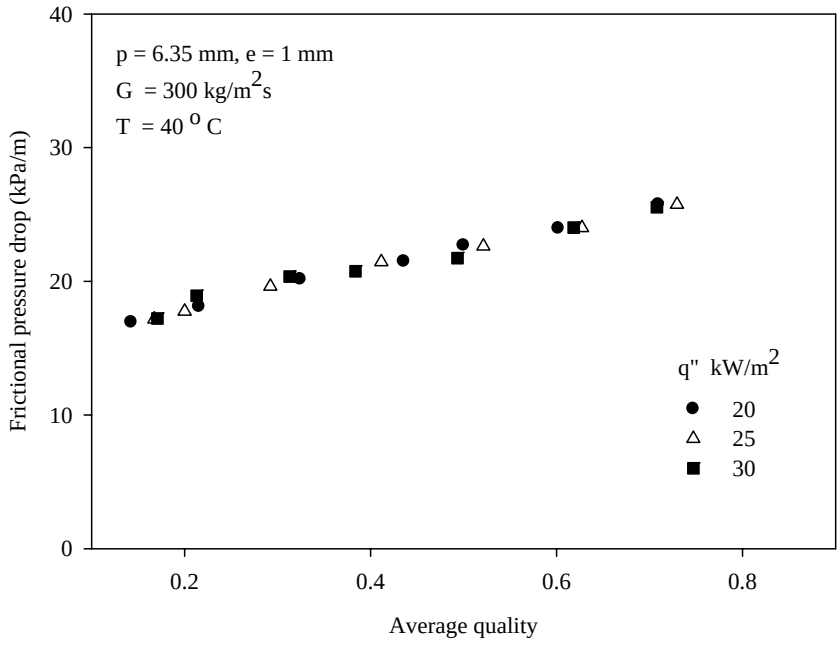

Figure 5.72 Effect of heat flux on condensation frictional pressure drop for a tube with p = 6.35 mm and e = 1 mm.

5.2.2.3 Effect of saturation temperature

The relationship between the frictional pressure drop and the average vapor quality at fixed values of heat flux and mass flux for different condensing temperatures of 40, 45, and 50 °C are illustrated in Figs. 5.73 and 5.74. It is observed that the increase of condensing temperature causes lower pressure drop. This phenomenon is due to the fact that when the condensing temperature increases, the specific volume of vapor decreases, which causes vapor velocity to decrease. As a result, the shear stress at the interface between the vapor and liquid film decreases. In addition, lower vapor velocity decreases the entrainment and redeposition of droplets, which in turn reduces the turbulence of fluid flow. The increase of condensing temperature also decreases the viscosity of liquid film, which results in lower flow resistance. For these reasons, the pressure drop tends to decrease as the condensing temperature increases.

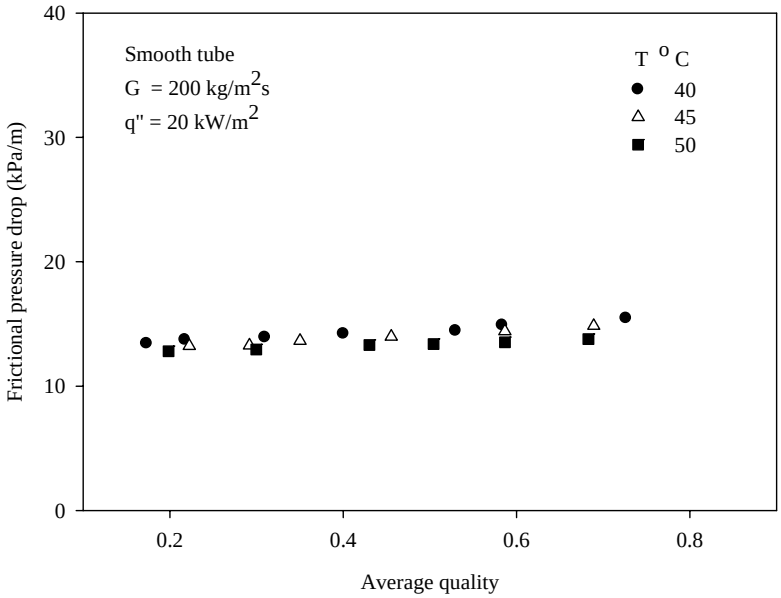

Figure 5.73 Effect of saturation temperature on condensation frictional pressure drop for a smooth tube.

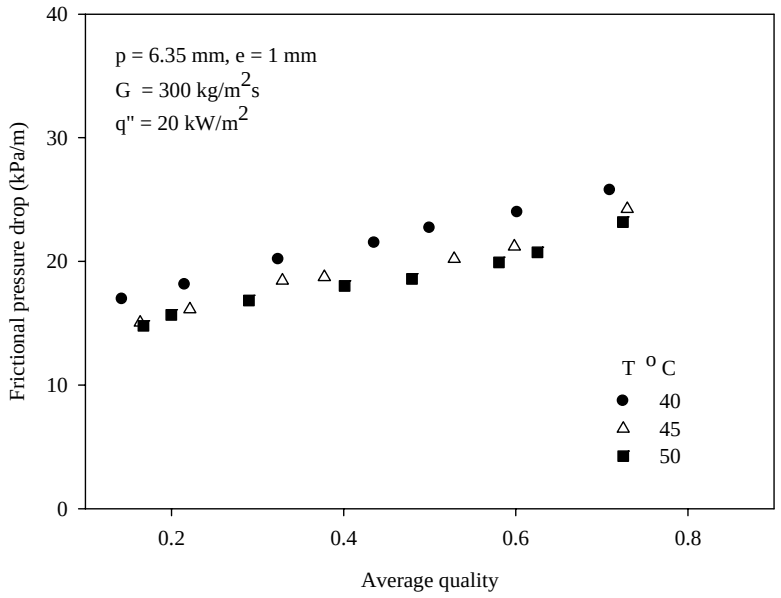

Figure 5.74 Effect of saturation temperature on condensation frictional pressure drop for a tube with p = 6.35 mm and e = 1 mm.

5.2.2.4 The comparison between smooth and corrugated tubes

The variation of the frictional pressure drop with average vapor quality in smooth and corrugated tubes are illustrated in Figs. 5.75-5.80. As seen from these figures, it is clear that the frictional pressure drop in the corrugated tube is higher than that in the smooth tube. This is because the rotational flow and turbulence augmentation are produced by the corrugation surface.

The effects of tube having different corrugation pitches at a constant corrugation depth of 1 mm on the frictional pressure drop are also shown in Figs. 5.75-5.77. The experimental results show that the frictional pressure drop increases as the corrugation pitch decreases. This is due to the fact that the lower corrugation pitch has higher corrugation surface which causes more turbulence and rotational flows. As a result, the pressure drop increases. The maximum frictional pressure drop enhancement is up to 70% for a pitch of 6.35 mm, 63% for a pitch of 8.46 mm and 53% for a pitch of 12.7 mm in comparison with the smooth tube at the mass flux of 400 kg/m^{2}s, heat flux of 20 kW/m^2 and saturation temperature of 40 °C.

In Figs. 5.78-5.80, the effects of the tube having different corrugation depths at a constant corrugation pitch of 12.7 mm on the frictional pressure drop are shown. It is observed that the frictional pressure drop in the tube having corrugation depth of 1 mm is higher than that in the tube having corrugation depths of 0.75 mm and 0.5 mm. The maximum value of frictional pressure drop enhancement is up to 53% for a depth of 1 mm in comparison with the smooth tube. For the tube having corrugation depths of 0.75 mm and 0.5 mm, the frictional pressure drop are nearly the same. These tubes increase the frictional pressure drop up to 43% in comparison with the smooth tube.

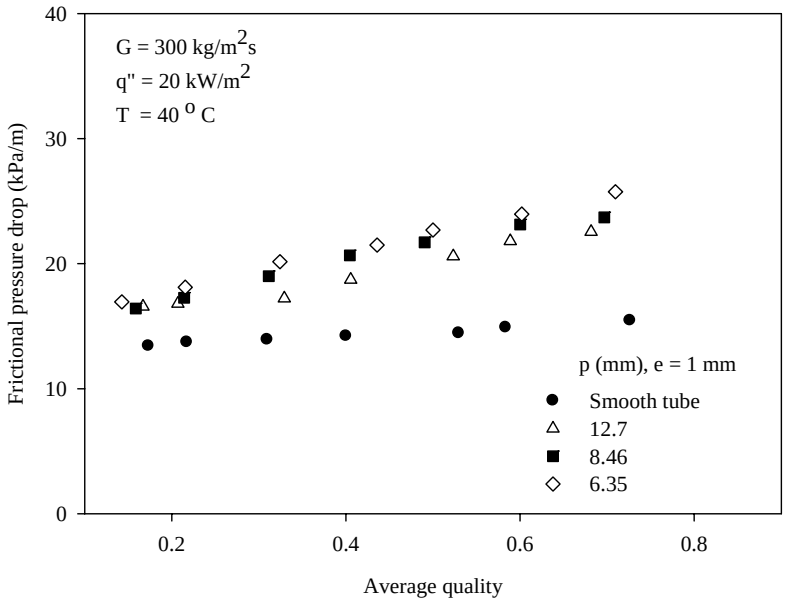

Figure 5.75 Effect of corrugation pitch on condensation frictional pressure drop for G = 300 kg/m^{2}s, q" = 20 kW/m^2 and T = 40 °C.

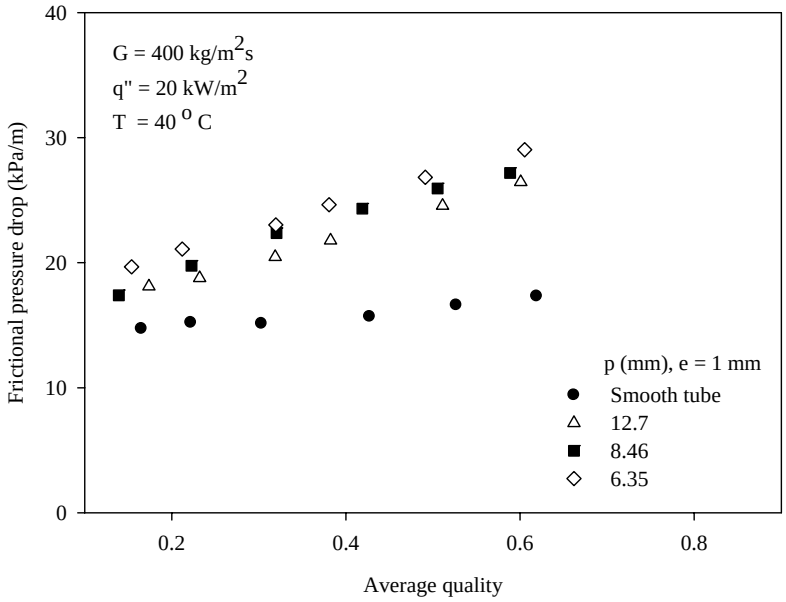

Figure 5.76 Effect of corrugation pitch on condensation frictional pressure drop for G = 400 kg/m^{2}s, q" = 20 kW/m^2 and T = 40 °C.

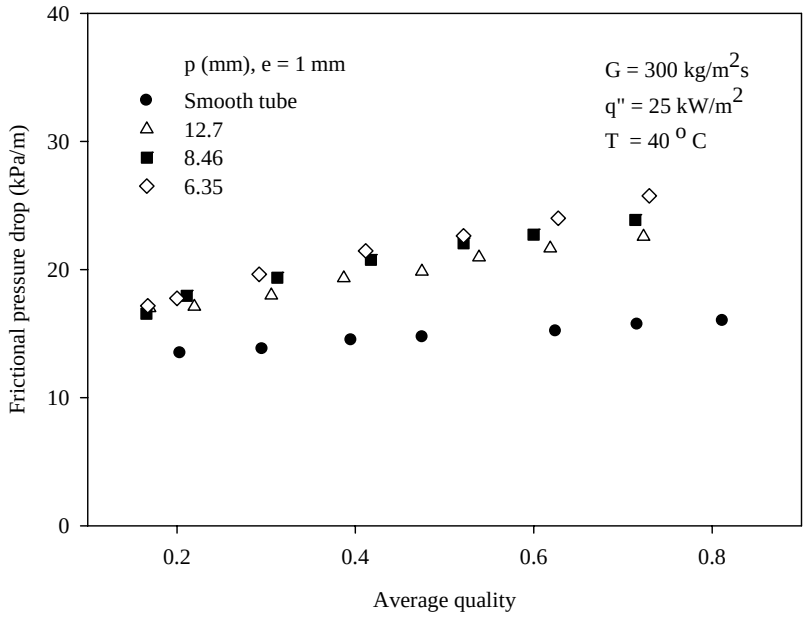

Figure 5.77 Effect of corrugation pitch on condensation frictional pressure drop for G = 300 kg/m^{2}s, q" = 25 kW/m^2 and T = 40 °C.

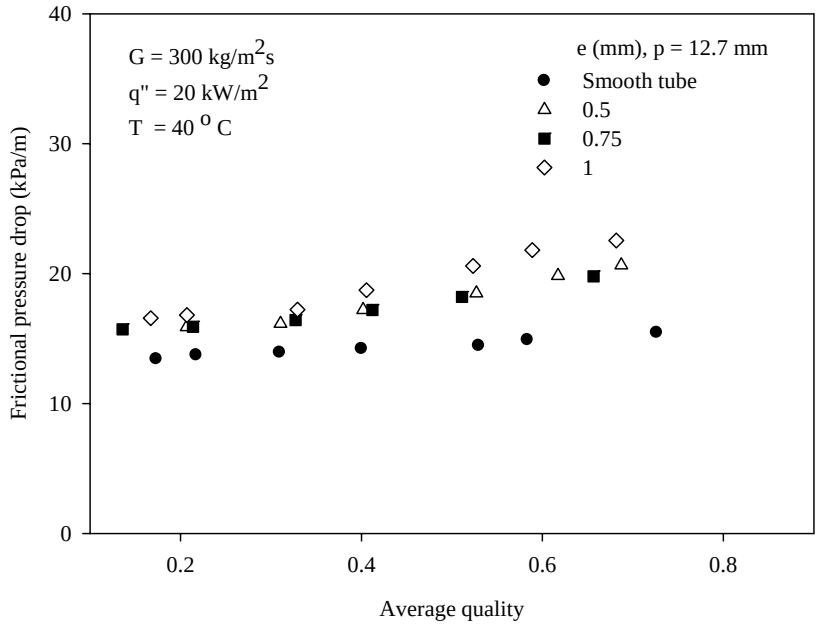

Figure 5.78 Effect of corrugation depth on condensation frictional pressure drop for G = 300 kg/m^{2}s, q" = 20 kW/m^2 and T = 40 °C.

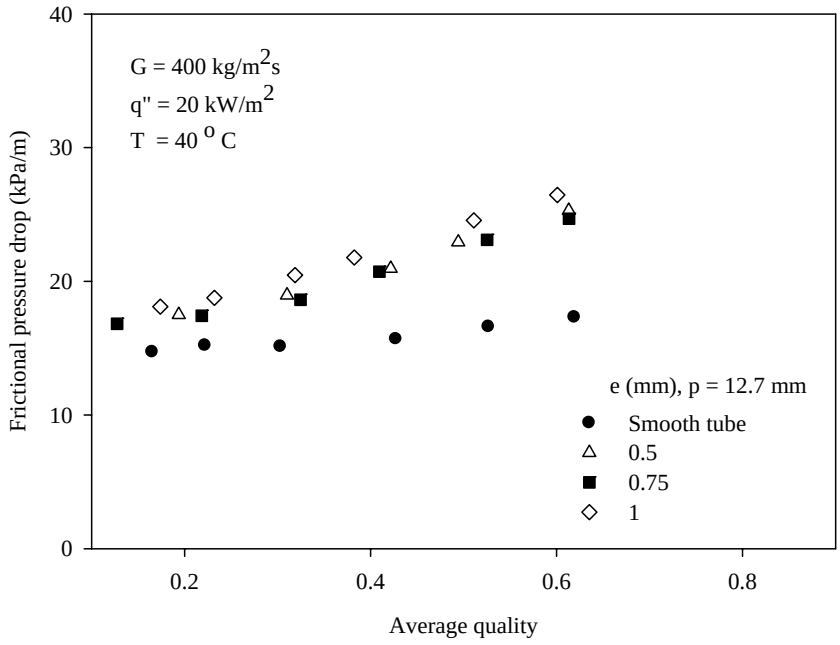

Figure 5.79 Effect of corrugation depth on condensation frictional pressure drop for G = 400 kg/m^{2}s, q" = 20 kW/m^2 and T = 40 °C.

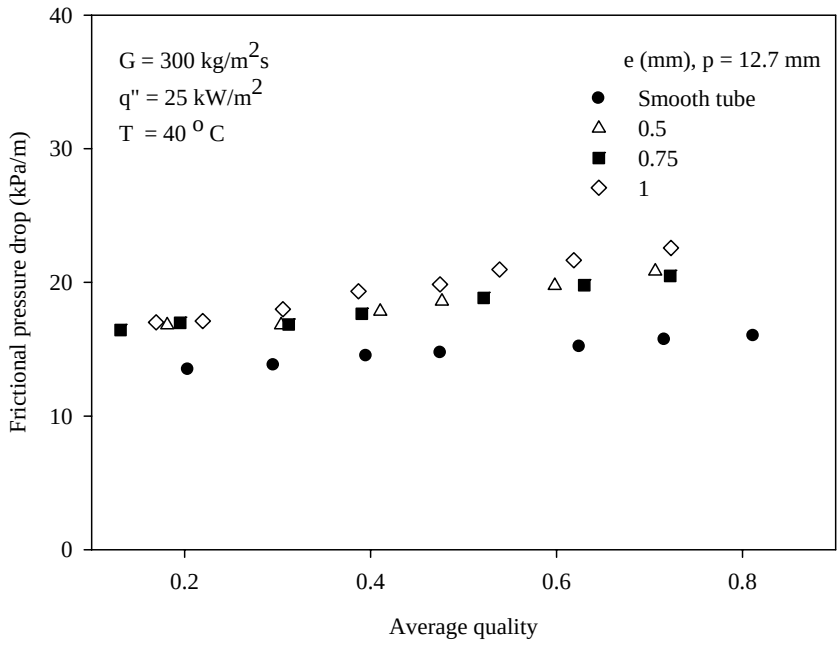

Figure 5.80 Effect of corrugation depth on condensation frictional pressure drop for G = 300 kg/m^{2}s, q" = 25 kW/m^2 and T = 40 °C.